Benchmarking on bifurcation and localization in J_2 plasticity for plane stress and plane strain conditions

M. Cervera
M. Chiumenti
D. Di Capua

Publication CIMNE Nº-370, December 2011

Benchmarking on bifurcation and localization in J_2 plasticity for plane stress and plane strain conditions

M. Cervera
M. Chiumenti
D. Di Capua

Publication CIMNE Nº-370, December 2011

International Center for Numerical Methods in Engineering
Gran Capitán s/n, 08034 Barcelona, Spain

Benchmarking on bifurcation and localization in J_2 plasticity for plane stress and plane strain conditions

M. Cervera, M. Chiumenti and D. Di Capua

International Center for Numerical Methods in Engineering (CIMNE)

Technical University of Catalonia (UPC)

Edificio C1, Campus Norte, Jordi Girona 1-3, 08034 Barcelona, Spain.

KEYWORDS: bifurcation, strain localization, incompressibility, plasticity, softening and stabilization.

Abstract

This paper studies the phenomenon of strain bifurcation and localization in J_2 plasticity under plane stress and plane strain conditions. Necessary conditions for the outcome of bifurcation, localization and decohesion are analytically established. It is shown that the explicit consideration of the bifurcation and decohesive limit conditions allows for the determination of localization angles in certain situations of interest that can be used to conduct benchmark tests on finite element formulations. The relative merits of irreducible, (stabilized) mixed and (displacement and/or strain) enhanced formulations are discussed. Numerical examples show that the mixed displacement/pressure formulation is to be preferred to the standard irreducible schemes in order to predict correct failure mechanisms with localized patterns of plastic deformation. Mixed elements are shown to be practically free from mesh directional bias dependence.

1 Introduction

Structural collapse is often the consequence of the formation of strain localization bands whose width is very small compared to the length scale of the structure. Depending on the material, the phenomena behind the formation of these bands may be diverse: concentration of micro-structural defects, intergranular slip, crystal dislocation, etc. In granular materials, strains concentrate in shear bands whose width is at most one order of magnitude larger than the grain size. In metals, dislocations occur at an even smaller scale. Therefore, from the structural point of view the localization band is perceived as a fracture surface of negligible width. It is generally accepted that the amount of energy released during the formation of a fracture unit area is a material property, called the fracture energy.

The question of modelling strain localization, formation of slip lines and subsequent structural collapse is a testing nonlinear problem in the field of computational mechanics. As with many other such challenges, solving real life, engineering problems can only be tackled by numerical procedures, such as the finite element method. Unfortunately, the results obtained in the initial attempts were bafflingly poor: either collapse mechanisms could not be numerically attained at all or if they could, they were strongly dependent on the mesh discretization used, both in terms of size and bias of the grid. In the last decades, many different finite element strategies have been tried on the issue, and the generated bibliography is voluminous.

The failure of the first attempts on the matter motivated studies directed to gain further insight in the subject of the necessary conditions for the occurrence of strain bifurcation and localization. The pioneering work by Hill [1] was taken up in more recent references ([2], [3], [4], [5], [6], [7], [8]). The outcome of these efforts was that the necessary conditions for bifurcation and localization of elasto-plastic materials were identified and formulae were obtained for the orientation of the shear bands to be expected in general circunstances. However, lack of a convincing reason for the failure of finite element simulations to reproduce the analytical results persisted.

Most of the studies regarding localization with J_2 plasticity have been carried out using the irreducible formulation, with the displacement field as the only primary variable. However, J_2 plastic flow is isochoric by definition, and for strain localization to take place the plastic regime has to be well developed and, then, the (incompressible) plastic component of the deformation is dominant over the elastic part. Displacement-based finite element irreducible

formulations are not well suited to cope with this quasi-incompressibility situation. The unsuitability of the irreducible formulation is more evident if low order finite elements are used which, conversely, are the first option when dealing with potentially discontinuous displacement and/or strain fields.

Reversely, the mixed displacement/pressure ($\mathbf{u}/p$) formulation is a much more appropriate framework to tackle (quasi)-incompressible problems [11]. However, it is not straight-forward to construct stable mixed low order elements, and one of the successful lines of research that allows to achieve this is the use of stabilization methods. In previous works ([12], [13], [14], [15], [16], [17] and [18]), the authors have used the orthogonal subgrid scale method to stabilize the mixed displacement-pressure method and applied it to the solution of incompressible elasto-plastic and damage problems. This stabilized framework leads to a discrete problem which is fully stable, free of pressure oscillations and volumetric locking and, thus, results obtained are not spuriously dependent on the directional bias of the finite element mesh.

The objectives of the present work are four-fold: (a) to revisit the analytical results on strain bifurcation and localization and to complement them with a more demanding decohesion condition that the localized solution must fulfil in the limit, (b) to clarify the specific difficulties encountered by low order finite element when dealing with strain localization problems and, particularly, with shear strain localization bands (c) to propose a series of benchmark problems in plane stress and plane strain situations for which the analytical solution is known and (d) to assess the relative performance of mixed and irreducible quadrilateral and triangular meshes in those benchmarks.

The outline of the paper is as follows. In Section 2, the mixed formulation for J_2 plasticity is sketched. In Section 3, the necessary conditions for strain bifurcation and localization are revised; analytical solutions for the localization angle under plane stress and plane strain conditions are obtained from the decohesion limit condition. In Section 4, the mechanical boundary value problem is stated in irreducible, mixed ($\mathbf{u}/p$) and stabilized mixed formulations. In Section 5, the approximability difficulties associated with strain localization problems are revised, discussing the role that displacement and/or strain enhancements may play. Section 6 presents results for a benchmark problem analyzed under plane stress and plane strain conditions with both irreducible and mixed elements. Finally, conclusions are drawn on the relative performance of the tested formulations.

2 J_2 plasticity constitutive model

For an elastoplastic model, the constitutive relation is expressed in total form as:

$$\boldsymbol{\sigma} = \mathbf{C} : (\boldsymbol{\varepsilon} - \boldsymbol{\varepsilon}^p) \tag{1}$$

where $\boldsymbol{\sigma}, \boldsymbol{\varepsilon}$ and $\boldsymbol{\varepsilon}^p$ are the (second-order) stress, strain and plastic strain tensors, and $\mathbf{C}$ is the (fourth-order) elastic tensor, which can be expressed as

$$\mathbf{C} = \left(K - \frac{2}{3} G \right) \mathbf{1} \otimes \mathbf{1} + 2G \, \mathbf{I} \tag{2}$$

where K is the bulk modulus, G is the shear modulus, $\mathbf{1}$ is the second-order identity tensor an $\mathbf{I}$ is the fourth-order symmetric identity tensor.

By definition, plastic flow in J_2 plasticity is purely deviatoric. In such circunstances, it is advantageous to introduce the following split of the stress tensor $\boldsymbol{\sigma}$ into its volumetric and deviatoric parts:

$$\boldsymbol{\sigma} = p\mathbf{1} + \mathbf{s} \tag{3}$$

where $p = \frac{1}{3} \operatorname{tr} \boldsymbol{\sigma}$ and $\mathbf{s} = \operatorname{dev} \boldsymbol{\sigma}$, are the pressure and the deviatoric stress, respectively.

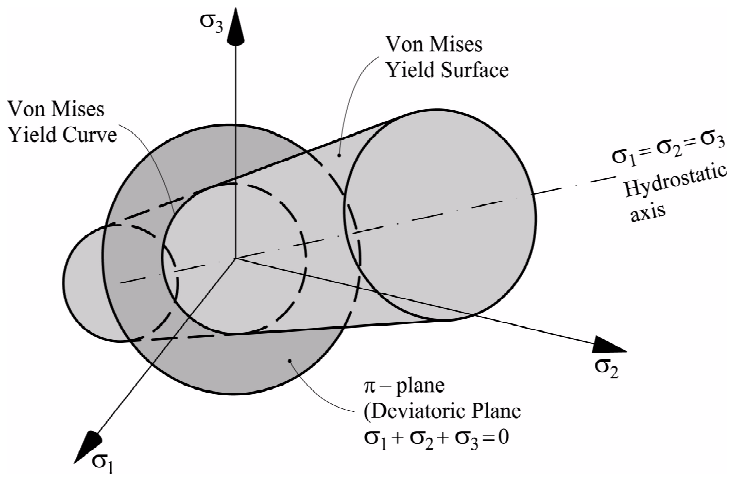

Figure 1: Yield surface for J_2 plasticity in the stress space

The strain tensor $\boldsymbol{\varepsilon} = \nabla^s \mathbf{u}$, where $\mathbf{u}$ are the displacements, is split analogously:

$$\boldsymbol{\varepsilon}(\mathbf{u}) = \frac{1}{3}\varepsilon_v \mathbf{1} + \mathbf{e} \tag{4}$$

where $\varepsilon_v = \operatorname{tr} \boldsymbol{\varepsilon} = \nabla \cdot \mathbf{u}$ and $\mathbf{e} = \operatorname{dev} \boldsymbol{\varepsilon}$, the volumetric and the deviatoric strain, respectively.

Correspondingly, the constitutive equation is split as:

$$p = K\varepsilon_v^e \tag{5a}$$

$$\mathbf{s} = 2G \operatorname{dev} \boldsymbol{\varepsilon}^e = 2G\mathbf{e}^e \tag{5b}$$

where ε_v^e and $\mathbf{e}^e = \mathbf{e} - \mathbf{e}^p$ are the elastic volumetric and the deviatoric parts of the strain tensor, respectively; $\mathbf{e}^p$ is the (deviatoric) plastic strain tensor. In J_2 plasticity, the volumetric part of plastic deformation is zero, so that $\varepsilon_v = \varepsilon_v^e = \nabla \cdot \mathbf{u}$.

Table 1 summarizes the J_2 elasto-plastic model used in this work, accounting for isotropic softening. The *equivalent plastic strain* is defined as $\xi = \sqrt{2/3} \int_o^t \|\dot{\mathbf{e}}^p\| \, dt$, and the equivalent von Mises stress is $\overline{s} = \sqrt{3/2} \, \|\mathbf{s}\|$.

The isotropic softening variable $r = r(\xi)$ defines the current size of the yield surface $\Phi(\mathbf{s}, r) = 0$, as it controls the value of the radius of the von Mises cylinder (depicted in Figure 1). Initially, when the equivalent plastic strain $\xi = 0$, r is equal to the initial flow stress σ_o. Along the softening regime r diminishes and, for large value of the equivalent plastic strain, it eventually vanishes.

The plastic multiplier $\dot{\gamma}$ is determined from the Kuhn-Tucker and consistency conditions. Details on how to efficiently integrate the J_2 elasto-plastic constitutive model can be found in reference [11].

For the bifurcation and localization analysis in the next Section, it is convenient to recall that Eq. (1) can also be expressed in rate form as:

$$\dot{\boldsymbol{\sigma}} = \mathbf{C}^{ep} : \dot{\boldsymbol{\varepsilon}} \tag{6}$$

where $\dot{\boldsymbol{\sigma}}$ and $\dot{\boldsymbol{\varepsilon}}$ are the (second-order) stress and strain rate tensors, and $\mathbf{C}^{ep}$ is the (fourth-order) elastic tensor, which, for associative plasticity, can be expressed as [11]:

$$\mathbf{C}^{ep} = \mathbf{C} - \frac{\mathbf{C} : \mathbf{m} \otimes \mathbf{m} : \mathbf{C}}{\mathbf{m} : \mathbf{C} : \mathbf{m} + \frac{2}{3}H} \tag{7}$$

where $\mathbf{m} = \partial\Phi / \partial\mathbf{s}$ is the second-order plastic flow tensor and the hardening/softening parameter is $H = H(\xi) = \partial r / \partial \xi$ (see Table 1).

1) Von Mises yield function, Φ:

$$\Phi(\mathbf{s}, r) = \|\mathbf{s}\| - \sqrt{\tfrac{2}{3}}\, r = \sqrt{\tfrac{2}{3}}\,(\overline{s} - r)$$

2) Isotropic softening variable, r:

$$r = \begin{cases} \sigma_o \left(1 - \frac{H_S}{\sigma_o}\xi\right) & 0 \le \xi \le \frac{\sigma_o}{H_S} \\ 0 & \frac{\sigma_o}{H_S} \le \xi \le \infty \end{cases} \qquad \text{linear softening}$$

$$r = \sigma_o \exp\left(-\frac{2H_S}{\sigma_o}\,\xi\right) \qquad 0 \le \xi \le \infty \qquad \text{exponential softening}$$

where ξ is the equivalent plastic strain, σ_o is the flow stress and $H_S > 0$ is the softening coefficient.

3) Plastic evolution laws:

$$\begin{aligned} \dot{\mathbf{e}}^p &= \dot{\gamma}\,\mathbf{m} \\ \dot{\xi} &= \dot{\gamma}\sqrt{\tfrac{2}{3}} \end{aligned}$$

where $\dot{\gamma}$ is the plastic multiplier and the plastic flow tensor $\mathbf{m} = \dfrac{\partial \Phi}{\partial \mathbf{s}} = \dfrac{\mathbf{s}}{\|\mathbf{s}\|}$ is normal to the yield surface.

Table 1: J_2 plastic constitutive model

With the definitions introduced above, the rate of deviatoric plastic work is $\dot{\mathcal{W}}^p = \mathbf{s} : \dot{\mathbf{e}}^p = \overline{s}\,\dot{\xi} = r\,\dot{\xi}$. Therefore, the total plastic work along a plastic process involving full softening, that is, from an elastic state $t = 0, \xi = 0, r = \sigma_o$, to a totally developed plastic state with $t = \infty, \xi = \infty, r = 0$, is equal to

$$\mathcal{W}^p_\infty = \int_{t=0}^{t=\infty} \dot{\mathcal{W}}^p dt = \int_0^\infty r\,(\xi)\, d\xi \; = \frac{\sigma_o^2}{2H_S} \tag{8}$$

both for linear or exponential softening.

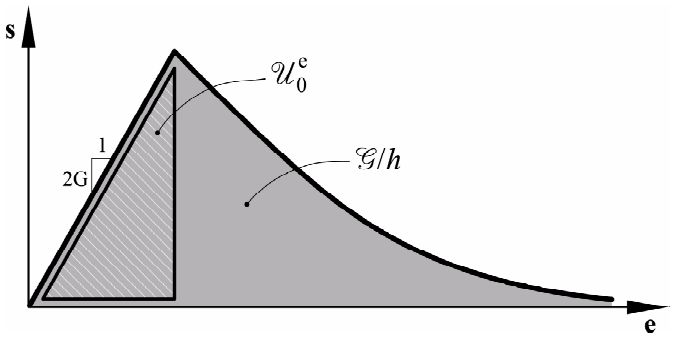

Figure 2: Stress-strain curve with exponential softening

Defining the elastic deviatoric strain energy at yielding as $\mathcal{U}_o^e = \sigma_o^2 / 2\,(2G)$ and the material brittleness number as $\Pi_B = \mathcal{U}_o^e / \mathcal{W}_\infty^p$, the softening parameter can be expressed as

$$H_S = 2G\ \Pi_B \tag{9}$$

Let us now assume that plastic dissipation localizes in a band of width b (see discussion in the next Section). Let us establish the requirements for this situation to be consistent with a limit case discrete model in which the strain energy is dissipated in a widthless discontinuity, say a slip line, and this dissipated energy per unit of slip line area is the fracture energy of the material $\mathcal{G}$.

The classical procedure ([19], [20], [21]), sketched in Figure 2, is as follows. The total energy dissipated during the fracture process per unit volume $\mathcal{D}$ within the localization band must fulfill the equation

$$\mathcal{D}\, b = \mathcal{G} \quad \Longrightarrow \quad \mathcal{D} = \frac{\mathcal{G}}{b} \tag{10}$$

For a plastic model, $\mathcal{D} = \mathcal{W}_\infty^p$, and, using Eqs. (8) and (9), this renders:

$$H_S = 2G\ \Pi_B = 2G\ \frac{\mathcal{U}_o^e}{\mathcal{G}\,/\,b}\ = 2G\ \frac{b}{\mathcal{L}} \tag{11}$$

where the length $\mathcal{L} = (\mathcal{G}\,/\mathcal{U}_o^e)$ is the *material length*, which depends only on the material properties. Eq. (11) makes the dimensional softening modulus H_S dependent on the ratio between the width of the localization band and the material length.

3 Bifurcation and localization analysis in J2 plasticity

3.1 Continuous, localized and discrete failure. Failure analysis

Let us consider a solid domain Ω subjected to a deformation evolution process leading to failure. Depending on the degree of continuity of the displacement and strain fields leading to full material deterioration, failure can be classified as ([6], [7], [8], [9]):

- **Continuous failure**: when the kinematic compatibility conditions of a continuum medium are preserved during the deformation and fracture process, that is, displacement and strain fields are continuous, displacement and strain jumps do not appear, $[\![\, \dot{\mathbf{u}} \,]\!] = 0, [\![\, \dot{\boldsymbol{\varepsilon}} \,]\!] = 0$.

- **Localized failure:** when the kinematic compatibility conditions of a continuum medium are not fulfilled by the strain field during the failure process, that is, the displacement is continuous, but strains are discontinuous, strain jumps do appear, $[\![\, \dot{\mathbf{u}} \,]\!] = 0, [\![\, \dot{\boldsymbol{\varepsilon}} \,]\!] \neq 0$.

- **Discrete failure:** when kinematic compatibility conditions are violated both by the displacement and strain fields to produce a fracture, that is, the displacement and strains are discontinuous, displacement and strain jumps do appear, $[\![\, \dot{\mathbf{u}} \,]\!] \neq 0, [\![\, \dot{\boldsymbol{\varepsilon}} \,]\!] \neq 0$.

For each type of failure to befall, there are necessary conditions that must be fulfilled. Analyzing the evolution of an increasing deformation process leading to failure (described by a stress-strain law such as the one depicted in Figure 2 for a point undergoing failure), several conditions can be identified that act as failure diagnostics, in the sense that they mark the occurrence of necessary requisites for a certain type of failure to be initiated. These are: the bifurcation condition, the localization condition and the decohesion condition. In the following, these requirements are discussed for the case of associative J_2-plasticity.

Bifurcation condition. This condition is usually associated to the stationarity of stress evolution with respect to the strain history, $\dot{\boldsymbol{\sigma}} = \mathbf{0}$. Because

of the rate Eq. (6), the stationary condition, or limit state, implies

$$\det \mathbf{C}^{ep} = 0 \tag{12}$$

Because positive definiteness of the constitutive tensor is invoked to prove solvability and uniqueness of the irreducible mechanical problem in incremental form, Eq. (12) is often called the *loss of uniqueness* condition. This name is not really appropriate as such condition would be met at an inflection point in the stress-strain relation if such point existed and that would *not* imply loss of uniqueness of the solution.

Loss of uniqueness is a necessary condition for *bifurcation* to take place, as it implies the existence of a limit or stationary stress point and two alternative solutions beyond that situation one solution in which all material points at the stationary level of stress proceed to deform forward (along a branch of the stress-strain curve with negative slope) and another solution in which some points deform forward and some others backward (unloading along the branch with positive slope). Therefore, the true necessary condition for (continuous or discontinuous) failure to materialize is that there exist strain rates $\dot{\boldsymbol{\varepsilon}}$, such that $\dot{\boldsymbol{\varepsilon}} : \dot{\boldsymbol{\sigma}} \leq \mathbf{0}$ and, therefore:

$$\dot{\boldsymbol{\varepsilon}} : \mathbf{C}^{ep} : \dot{\boldsymbol{\varepsilon}} \leq 0 \tag{13}$$

Note that Eq. (12) is obtained by restricting Eq. (13) to the equality case.

Localization condition. This condition detects the possibility of formation of spatial discontinuities along material surfaces defined by a normal vector $\mathbf{n}$. The condition applies both to weak (strain) as to strong (strain and displacement) discontinuities depending on the severity of the jumps in the kinematic fields.

Consider the body Ω, as shown in Figure 3, crossed by a discontinuity S. Regions Ω^+ and Ω^- are the parts of the body located "in front" and "behind" S. Consider, as in Figure 3a.1, that S^+ and S^- are two lines that run parallel to S, at a relative distance b. Surfaces S^+ and S^-delimit a localization band of width b where strain localization may occur.

Let $\mathbf{w} = \mathbf{u}^+ - \mathbf{u}^-$ be the difference between the displacement "in front" and "behind" the localization band and $\boldsymbol{\beta} = \mathbf{w} \,/\, b$ be a deformation vector defined with respect to b. The top graph in Figure 3a.2 shows a certain displacement component along a line normal to S, with the jump $\mathbf{w}$ occurring continuously between S^- and S^+. The strain corresponding to the variation

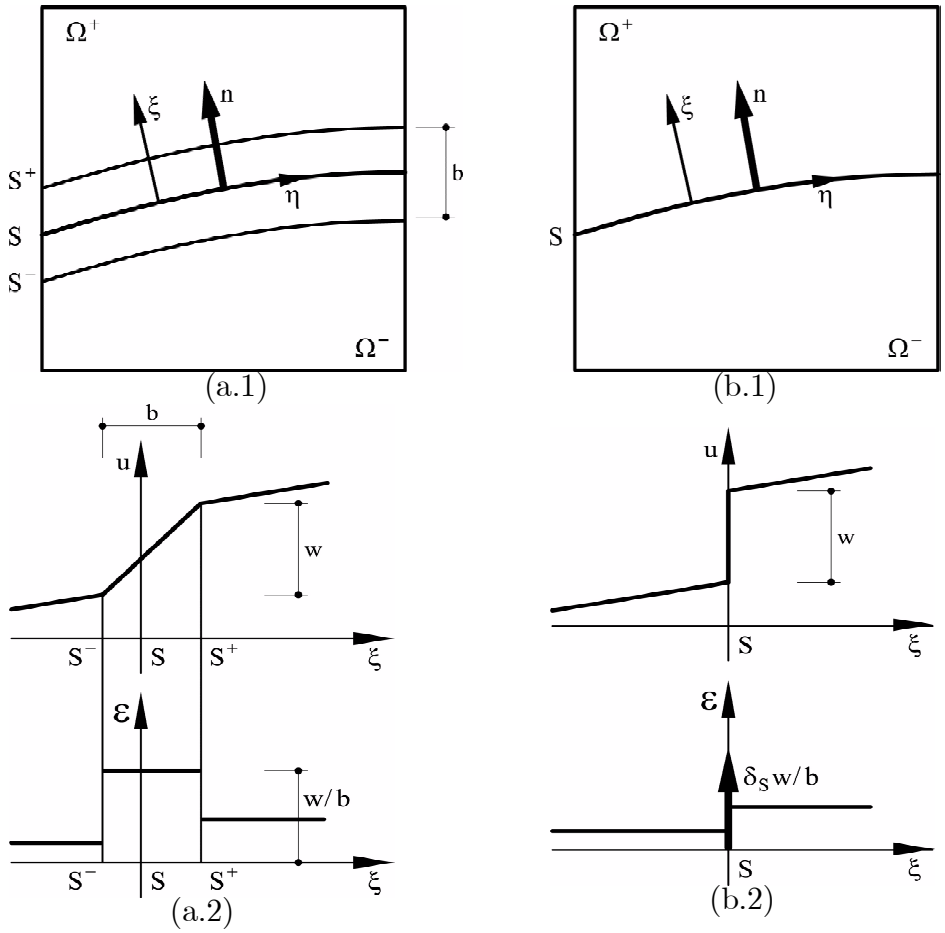

Figure 3: Localized failure: (a) weak and (b) strong discontinuities

of the displacement along the line normal to S is shown in the bottom graph. The behaviour inside the localization band is established through a softening stress-strain law like the one in Figure 2.

Let us now consider the case of strong discontinuities. Note that such case can be formally constructed from the one previously discussed of a localization band of width b comprised between two weak discontinuities simply by taking the limit $b \to 0$. In this case, as shown in Figure 3b.1, the weak discontinuities at lines S^+ and S^- converge to a strong discontinuity at line S. Now, $\mathbf{w} = \mathbf{u}^+ - \mathbf{u}^- = [\![\, \mathbf{u} \,]\!]$, the difference between the displacement rates "in front" and "behind" the discontinuity line, is a real displacement jump; the deformation vector $\dot{\boldsymbol{\beta}} = \lim_{b \to 0} \mathbf{w} \,/\, b$ is not only discontinuous but unbounded

(see Figure 3b.2). The behaviour of such a strong discontinuity must be established via a discrete softening traction-jump law or, through a *regularized* softening stress-strain law like in the previous case of a localization band [21].

Reversely, a localization band of width b bounded by two weak discontinuities can be viewed as a regularized strong discontinuity, and the corresponding softening stress-strain law as a regularization of a certain discrete traction-displacement jump law. This is the standpoint behind the softening regularization procedure described in Section 2 and the one that will be pursued throughout this work.

According to Maxwell's compatibility condition, the jump in the strain field between the inside and the outside of the localization band can be expressed as $[\![\, \dot{\boldsymbol{\varepsilon}} \,]\!] = (\mathbf{n} \otimes \dot{\boldsymbol{\beta}})^{\mathrm{s}}$. According to Cauchy's theorem, the jump on the variation of tractions, $\dot{\mathbf{t}} = \mathbf{n} \cdot \dot{\boldsymbol{\sigma}}$ across the discontinuity lines S^+ and S^- must be null, $[\![\, \dot{\mathbf{t}} \,]\!] = \mathbf{0}$. Assuming a linear comparison solid, this is shown to imply the singularity of the (second-order) acoustic tensor $\mathbf{Q}^{ep} = \mathbf{n} \cdot \mathbf{C}^{ep} \cdot \mathbf{n}$:

$$\det \mathbf{Q}^{ep} = 0 \tag{14}$$

The occurrence of this condition for a given pair $\mathbf{n}$ and $\mathbf{C}^{ep}$ implies the *loss of material ellipticity* of the constitutive relation and this is a necessary condition for the appearance of *weak discontinuities* and *localized failure* to take place. Eq. (14) is also called *discontinuous bifurcation condition.*

Classically, the problem of determining the onset of the discontinuous bifurcation consists in finding the first instant of the loading process (maximum value of the softening parameter $H = H_{cr}$) and the corresponding orientation of the discontinuity $\mathbf{n}_{cr}$ that satisfy that $\det \mathbf{Q}^{ep}(H_{cr}, \mathbf{n}_{cr}) = 0$.

Condition (14) is not very stringent. A situation exhibiting neutral loading inside and outside the localization band would meet it, without being really a localization scenario.

This point deserves some additional discussion. Following reference [7], let us require that for the localization band to form and in subsequent instants, material points inside the band undergo plastic loading ($\dot{\gamma} \geq 0$) while points outside the band unload elastically ($\dot{\gamma} = 0$). If $\dot{\bar{\boldsymbol{\varepsilon}}}$ is the regular (unloading) strain rate which is common to the points outside and inside the localization band, the corresponding stress rates are:

$$\dot{\boldsymbol{\sigma}}_{\mathrm{ext}} = \mathbf{C} : \dot{\boldsymbol{\varepsilon}}_{\mathrm{ext}} = \mathbf{C} : \dot{\bar{\boldsymbol{\varepsilon}}} \tag{15a}$$

$$\dot{\boldsymbol{\sigma}}_{\mathrm{int}} = \mathbf{C} : (\dot{\boldsymbol{\varepsilon}}_{\mathrm{int}} - \dot{\boldsymbol{\varepsilon}}^p) = \mathbf{C} : \left(\dot{\bar{\boldsymbol{\varepsilon}}} + (\mathbf{n} \otimes \dot{\boldsymbol{\beta}})^{\mathrm{s}} - \dot{\gamma}\, \mathbf{m} \right) \tag{15b}$$

where $[\![\, \dot{\boldsymbol{\varepsilon}} \,]\!] = \dot{\boldsymbol{\varepsilon}}_{\text{int}} - \dot{\boldsymbol{\varepsilon}}_{\text{ext}} = (\mathbf{n} \otimes \dot{\boldsymbol{\beta}})^{\text{s}}$ is the difference in the total strain rate, and the plastic strain rate is $\dot{\boldsymbol{\varepsilon}}^p = \dot{\gamma}\, \mathbf{m}$ ($\dot{\gamma}$ is the plastic multiplier and $\mathbf{m}$ is the plastic flow tensor). Therefore, the jump in the stress rate is:

$$[\![\, \dot{\boldsymbol{\sigma}} \,]\!] = \dot{\boldsymbol{\sigma}}_{\text{int}} - \dot{\boldsymbol{\sigma}}_{\text{ext}} = \mathbf{C} : \Big((\mathbf{n} \otimes \dot{\boldsymbol{\beta}})^{\text{s}} - \dot{\gamma}\, \mathbf{m} \Big) \tag{16}$$

Substituting, the traction equality, $[\![\, \dot{\mathbf{t}} \,]\!] = \mathbf{n} \cdot [\![\, \dot{\boldsymbol{\sigma}} \,]\!] = \mathbf{0}$, reads:

$$\mathbf{n} \cdot \Big[\mathbf{C} : \Big((\mathbf{n} \otimes \dot{\boldsymbol{\beta}})^{\text{s}} - \dot{\gamma}\, \mathbf{m} \Big) \Big] = \mathbf{0} \tag{17}$$

and this is an alternative stating of the discontinuous bifurcation condition in Eq. (14). Defining the elastic acoustic tensor as $\mathbf{Q} = \mathbf{n} \cdot \mathbf{C} \cdot \mathbf{n}$ and making use of the symmetries of tensor $\mathbf{C}$, Eq. (17) determines uniquely the deformation vector rate $\dot{\boldsymbol{\beta}}$ as:

$$\dot{\boldsymbol{\beta}} = \dot{\gamma}\, \mathbf{Q}^{-1} \ (\mathbf{m} : \mathbf{C} \cdot \mathbf{n}) \tag{18}$$

Let us now require, as said, that material points outside the band unload elastically, that is:

$$\mathbf{m} : \dot{\boldsymbol{\sigma}}_{\text{ext}} \leq 0 \tag{19}$$

while points inside the band comply with the plastic consistency condition, $\dot{\Phi} = 0$:

$$\dot{\Phi} = \frac{\partial \Phi}{\partial \boldsymbol{\sigma}} : \dot{\boldsymbol{\sigma}} + \frac{\partial \Phi}{\partial r}\, \dot{r} \tag{20a}$$

$$= \mathbf{m} : \dot{\boldsymbol{\sigma}}_{\text{int}} - \frac{2}{3}\, \dot{\gamma}\, H = 0 \tag{20b}$$

Using this result and Eq. (16), Eq. (19) can be rewritten as:

$$\frac{2}{3}\, \dot{\gamma}\, H \leq \mathbf{m} : \mathbf{C} : \Big[(\mathbf{n} \otimes \dot{\boldsymbol{\beta}})^{\text{s}} - \dot{\gamma}\, \mathbf{m} \Big] \tag{21}$$

Substituting (18) in (21), yields [7]:

$$H \leq \frac{3}{2} \left[\mathbf{a} : \mathbf{Q}^{-1} : \mathbf{a} - \mathbf{m} : \mathbf{C} : \mathbf{m} \right] \tag{22}$$

where $\mathbf{a} = \mathbf{m} : \mathbf{C} \cdot \mathbf{n}$. Eq. (21) determines the maximum value of the softening parameter that allows for strain localization with a discontinuous strain field. We will refer to Eq. (21) as the *localization condition*. Note that Eq. (14) is obtained by restricting Eq. (21) to the equality case.

Incidentally, let us remark that any softening law designed to allow full decohesion across the localization band at the end of the straining process (for $\|\boldsymbol{\varepsilon}\| \to \infty$) must be such that the softening parameter $H = 0$ in the limit, as shown in Figure 2. This means that, whatever happens before, the softening parameter H must increase during the final stages of the deformation process, from negative values to zero, asymptotically (like in exponential softening) or abruptly (like in linear softening). Therefore, if condition (21) is not met at the initial stages of the deformation process, say at yielding, and the localization condition is fulfilled at a later stage of the deformation process, it will be because plastic flow will make the right hand side of the inequality increase at a faster rate than the left hand side, which be increasing as well.

Decohesion condition. This condition reflects the necessity of having null rate of traction at the discontinuity (weak or strong) at the end of the straining process, that is

$$\lim_{\|\boldsymbol{\varepsilon}\| \to \infty} \dot{\mathbf{t}} = \mathbf{0} \tag{23}$$

As $\dot{\mathbf{t}} = \mathbf{n} \cdot \dot{\boldsymbol{\sigma}}$, Eq. (23) implies that, in the limit $\|\boldsymbol{\varepsilon}\| \to \infty$, $\dot{\boldsymbol{\sigma}} = \dot{\boldsymbol{\sigma}}_{\text{ext}} = \dot{\boldsymbol{\sigma}}_{\text{int}} = \mathbf{0}$. Because of Eq. (15a), the condition $\dot{\boldsymbol{\sigma}}_{\text{ext}} = \mathbf{0}$ implies that, in the decohesion limit, the regular (unloading) strain rate $\dot{\bar{\boldsymbol{\varepsilon}}}$ vanishes and then, Eq. (15b), the condition $\dot{\boldsymbol{\sigma}}_{\text{int}} = \mathbf{0}$ implies that, in the limit, the plastic tensor has the structure dictated by Maxwell's compatibility condition:

$$(\mathbf{n} \otimes \dot{\boldsymbol{\beta}})^{\text{s}} = \dot{\gamma}\, \mathbf{m} \tag{24}$$

or, in other words, it implies that, in the limit $\|\boldsymbol{\varepsilon}\| \to \infty$, the localized strain rate field is purely plastic (inelastic in a general case).

Remark 1 *Eq. (24) is different from Eq. (21), in the sense that it is much more constrictive in the possibilities for the orientation* $\mathbf{n}$*. Consequently, it does not follow from the fact that a given discontinuity orientation* $\mathbf{n}$ *satisfies the localization condition* $\det \mathbf{Q}^{ep}(H, \mathbf{n}) = 0$ *for a given maximum (negative)* $H < 0$ *value, that the same orientation* $\mathbf{n}$ *will in the limit* $\|\boldsymbol{\varepsilon}\| \to \infty$ *satisfy the decohesion condition, with* $H = 0$*. In other words, it does not follow from the fact that a certain discontinuity can form at an orientation given by Eq. (21) that such discontinuity can reach the decohesion limit.*

Remark 2 *Reversely, the condition* $\dot{\boldsymbol{\sigma}} = \mathbf{0}$ *(for* $\|\boldsymbol{\varepsilon}\| \to \infty$*, in the final stages of the deformation process) from which Eq. (24) follows is exactly the*

same stationary condition $\dot{\boldsymbol{\sigma}} = \mathbf{0}$ *in Eq. (12), necessary for the existence of a limit point and the initiation of strain bifurcation,* plus *the compatibility requirement that the difference in the rate of the strain field satisfies Maxwell's condition,* $[\![\, \dot{\boldsymbol{\varepsilon}} \,]\!] = (\mathbf{n} \otimes \dot{\boldsymbol{\beta}})^{s}$.

Remark 3 *Hence, Eq. (24) is the* necessary *and* sufficient *condition for the occurrence of bifurcation and localization of the strain field and decohesion in the limit case along a localization band (or a regularized strong discontinuity) with orientation* $\mathbf{n}$. *This is why the term* strong discontinuity condition *was used in reference [8] for it. However, the decohesion condition, like the localization condition, applies both to weak and strong discontinuities alike.*

Remark 4 *From the previous Remarks and because the localization band is bounded by material surfaces, it follows that Eq. (24)* must hold all along the localization process, *for the decohesive limit to be reached.*

Remark 5 *The physical interpretation of this condition is simple: all of the difference in the strain field between the interior and the exterior points of the localization band must be inelastic (plastic in this case).*

Remark 6 *For a given plastic flow tensor* $\mathbf{m}$ *(and plastic multiplier* $\dot{\gamma}$*), Eq. (24) determines the orientation of the discontinuity* $\mathbf{n}$ *(and the rate of the deformation vector* $\dot{\boldsymbol{\beta}}$*). This is exploited in the next Section. However, the solution for the corresponding (nonlinear) equations may be not uniquely determined or may not exist.*

Remark 7 *The orientation of the discontinuity* $\mathbf{n}$ *derived from Eq. (24) does not depend on the elastic properties. It depends only on the plastic yield surface adopted and the stress state.*

3.2 Orientation of the discontinuity

The question of determining the orientation of the material surface exhibiting strain (in the weak discontinuity case) or displacement (in the strong discontinuity case) jumps has been object of some attention in the literature.

Several authors have found analytical solutions for the *localization condition,* Eq. (21). In reference [2], analytical expressions for the orientation of $\mathbf{n_{cr}}$ are obtained for tridimensional cases by means of the spectral analysis of the acoustic tensor $\mathbf{Q}$ and using Lagrange multipliers. In [3] two-dimensional

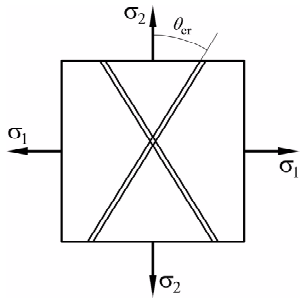

Figure 4: Definition of critical localization angle

problems are analyzed by maximizing a convenient second-degree polynomial scalar function. In [4], bifurcation orientations are found for some particular cases of J_2 plasticity by direct eigen-analysis of $\mathbf{Q}$. References [5] and [6] obtained a geometrical solution for the problem in the plane stress and plane strain cases. Finally, references [7] and [8] tackled the problem within the context of the strong discontinuity approach.

In this work, a different approach is adopted. Attention will be restricted to cases of J_2 associative plasticity under plane stress and plane strain condition. In this cases, analytical expressions for the orientation of localization bands for which the *decohesion condition,* Eq. (23), rather than the localization condition, Eq. (21), can be fulfilled are easy to obtain.

In the following, an orthonormal base $\{\mathbf{n}, \mathbf{t}, \mathbf{p}\}$ is used, with $\mathbf{n}$ normal to the surface S, $\mathbf{t}$ tangent to it and on the plane of interest and $\mathbf{p}$ orthogonal to the plane of the problem. In this base, the deformation vector rate can be expressed as $\dot{\boldsymbol{\beta}} = \dot{\beta}_n \mathbf{n} + \dot{\beta}_t \mathbf{t}$.

3.2.1 Plane stress conditions

In plane stress conditions, the out of plane components of the strain tensor need not be explicitly considered, since $\sigma_3 = 0$ [11]. Then, the decohesion condition can be expressed in the base $\{\mathbf{n}, \mathbf{t}, \mathbf{p}\}$ directly as

$$\begin{bmatrix} \dot{\beta}_n & \frac{1}{2}\dot{\beta}_t \\ \frac{1}{2}\dot{\beta}_t & 0 \end{bmatrix} = \dot{\gamma} \begin{bmatrix} m_{nn} & m_{nt} \\ m_{nt} & m_{tt} \end{bmatrix} \tag{25}$$

Therefore, the actual condition can be stated as:

$$m_{tt} = 0 \tag{26}$$

Let m_1, m_2 ($m_1 > m_2$) and $\mathbf{e}_1$, $\mathbf{e}_2$ be the principal eigen values and the principal directions of the plastic flow tensor $\mathbf{m}$, respectively. Let θ be the angle of $\mathbf{n}$ with respect to $\mathbf{e}_1$, so that $\mathbf{n} = \cos\theta\,\mathbf{e}_1 + \sin\theta\,\mathbf{e}_2$. Then the component m_{tt} can be expressed as

$$m_{tt} = (m_1 - m_2)\sin^2\theta + m_2 \tag{27}$$

From Eqs. (26) and (27) the critical angle (see Figure 4 for its definition) can be computed as:

$$\sin^2\theta_{cr} = -\frac{m_2}{m_1 - m_2} \tag{28}$$

Note that Eq. (28) provides for two opposite values for angle θ_{cr}. Note also that there are stress combinations, for instance, with $m_1 > m_2 > 0$, for which $\sin\theta_{cr} > 1$, and localization with decohesion is impossible.

Alternatively, Eq. (28) may be written as:

$$\tan^2\theta_{cr} = -\frac{m_2}{m_1} = \tan\tilde{\theta} \tag{29}$$

where $\tilde{\theta}$ is the angle between the projection of the flow vector (normal to the yields surface cylinder) and the principal axis σ_1 axis (see Figure 5).

In the case of J_2 plasticity, it is verified that $m_i = s_i$, where s_i are the deviatoric principal stresses.

Using these results, Table 2 can be obtained for the critical orientations in different plane stress load combinations.

	Stress components			Critical angle θ_{cr}
		σ_1	σ_2	
Plane stress	**P1** Pure Shear	1.0	-1.0	45.00°
	P2 Uniaxial Tension	1.0	0.00	35.26°
	P3 Biaxial Tension 1	1.0	0.25	21.80°
	P4 Biaxial Tension 2	1.0	0.50	0.00°

Table 2: Localization angles for plane stress

In a plane stress state, the bifurcation and localization conditions are both fulfilled at the onset of yielding. Therefore, softening and localization occur immediately after the yield surface is reached for the first time. At that instant, it also happens that plastic flow is in the direction required for the decohesion condition to be eventually met.

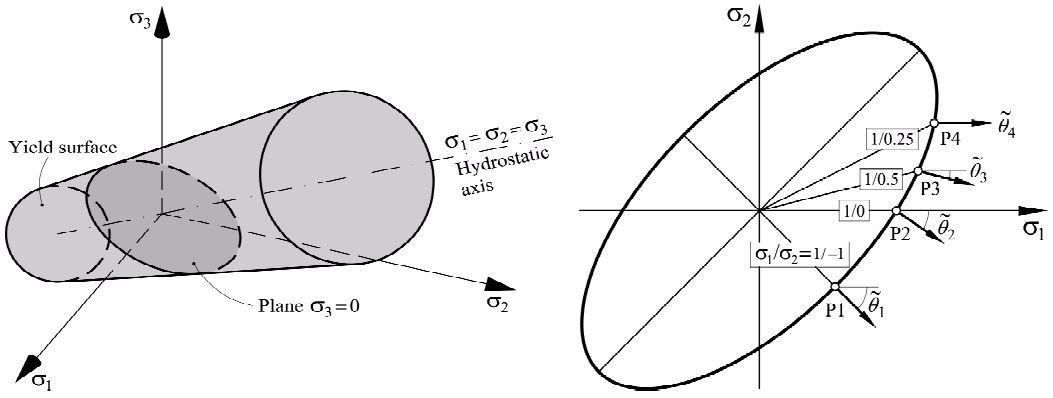

Figure 5: Locus and flow directions and localization angles in plane stress conditions

It is clear from Figure 5 that bifurcation of the strain field after yielding consists on the points inside the localization band undergoing further straining in the direction of the plastic flow, while the points outside the localization band unload elastically. For the pure shear case, **P1**, bifurcation and localization befall without the need of strain rotation, because the direction of plastic flow coincides with the direction of elastic loading/unloading. However, for the other investigated stress combinations, **P2** (uniaxial straining)**, P3** and **P4** (mixed loading), a significant amount of reorientation of the principal strain directions takes place during the localization process. They have to rotate from being coaxial with the principal stress directions at the instant of yielding to be totally aligned with the plastic flow to be able to meet the decohesion condition.

3.2.2 Plane strain conditions

Under plane strain conditions, the decohesion condition in the base $\{\mathbf{n}, \mathbf{t}, \mathbf{p}\}$ is

$$\begin{bmatrix} \dot{\beta}_n & \frac{1}{2}\dot{\beta}_t & 0 \\ \frac{1}{2}\dot{\beta}_t & 0 & 0 \\ 0 & 0 & 0 \end{bmatrix} = \gamma \begin{bmatrix} m_{nn} & m_{nt} & 0 \\ m_{nt} & m_{tt} & 0 \\ 0 & 0 & m_{pp} \end{bmatrix} \tag{30}$$

From this, it must be $m_{tt} = 0$, and then, as for the plane stress case, it follows that:

$$\tan^2 \theta_{cr} = -\frac{m_2}{m_1} \tag{31}$$

	Stress components			Critical angle θ_{cr}
		σ_1	σ_2	
Plane strain	**P1** Pure Shear	1.0	-1.0	45.0°
	P2 Uniaxial Tension	1.0	0.00	45.0°
	P3 Biaxial Tension 1	1.0	0.25	45.0°
	P4 Biaxial Tension 2	1.0	0.50	45.0°

Table 3: Localization angles for plane strain

But, in this case, due to the plane strain constraint $\varepsilon_{pp} = 0$ and the flow rule $\dot{\boldsymbol{\varepsilon}}^p = \dot{\gamma}\,\mathbf{m}$, the limit decohesion condition $\dot{\boldsymbol{\sigma}} = \mathbf{0}$ implies $\dot{\boldsymbol{\varepsilon}} = \dot{\boldsymbol{\varepsilon}}^p$ and:

$$m_{pp} = 0 \tag{32}$$

Taking into account that for a purely deviatoric flow $m_{pp} = m_3 = s_3 = -(s_1 + s_2)$ and $m_i = s_i$, Eq. (32) implies that in the decohesive limit

$$s_3 = 0 \Rightarrow s_1 = -s_2 \Rightarrow m_1 = -m_2 \tag{33}$$

Replacing condition (33) into expression (31) it is concluded that the localization angle in plane strain condition is always $\theta_{cr} = 45.0°$, irrespective of the stress loading conditions (see Table 3).

For a geometrical interpretation of the critical angle θ_{cr}, consider that the decohesion condition $s_3 = 0$ implies that the equality $\sigma_1 + \sigma_2 = 2\sigma_3$ holds. This means that the cohesion condition can only be met at the intersection of the yield cylinder and the plane $\sigma_1 + \sigma_2 = 2\sigma_3$, which is a plane that contains the hydrostatic axis $\sigma_1 = \sigma_2 = \sigma_3$ and the line $\sigma_1 + \sigma_2 = 0$ in the $\sigma_3 = 0$ plane. This intersection is composed of two lines parallel to the hydrostatic axis, whose projections in the $\sigma_1 - \sigma_2$ plane are two parallel lines at $\tilde{\theta} = 45°$ with the σ_1 axis (see Figure 6).

The intrinsic restriction $\varepsilon_{pp} = 0$ that defines the plane strain condition deserves an additional comment. The limit condition $\dot{\boldsymbol{\sigma}} = \mathbf{0}$, which implies $m_{pp} = 0$, does not only apply to the decohesion limit, but also to the bifurcation condition itself, necessary for a softening response to take place. This means that, unlike what happens under plane stress situations, bifurcation does not commonly coincides with the onset of yielding. In general, substantial rotation of the principal strain directions has to take place from the onset of plastic behavior (where principal directions of strain and stress coincide and principal values are proportional), to the limit point where softening behavior may be initiated (where neither of the previous conditions

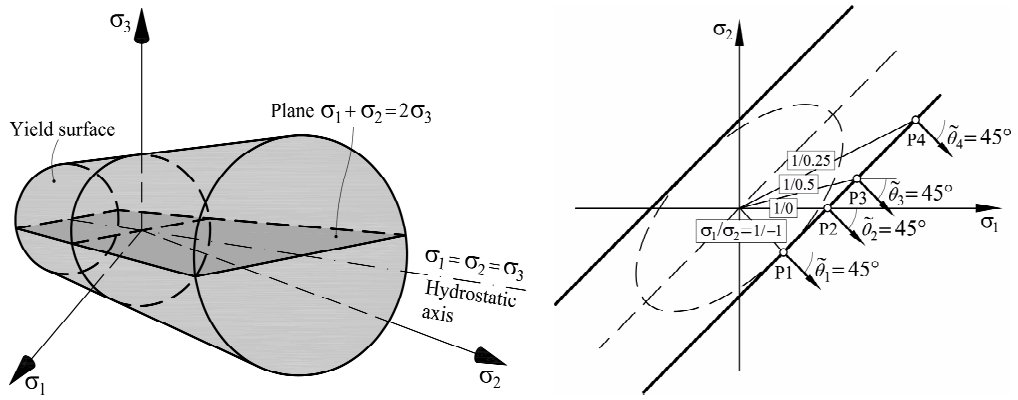

Figure 6: Locus and flow directions and localization angles in plane strain conditions

happen). Only for pure shear, point **P1** in Figure 6, it is $\varepsilon_{tt} = \varepsilon_{pp} = 0$ in the elastic range, and thus yielding and bifurcation may happen at the same time (in fact, the pure shear case complies both with the plane stress and plane strain requirements). For the other investigated stress combinations, **P2** (uniaxial straining)**, P3** and **P4** (mixed loading), stress will continue to rise under increasing strain after plastic flow. Only when a certain amount of plastic behaviour has come about, with the corresponding reorientation of the principal strain directions, the localization process is set in motion. This reorientation is larger the more the yielding state differs from pure shear.

Note that the expression for the localization angle found both plane stress and strain conditions, $\tan^2 \theta_{cr} = -(s_2 \,/\, s_1)$, does not depend on the elastic constitutive tensor $\mathbf{C}$: it is independent of the elastic material properties.

4 Irreducible, mixed and stabilized formulations

The strong form of the continuum elasto-plasticity problem can be stated as: given the elastic tensor $\mathbf{C}$ and prescribed body forces $\mathbf{f}$, find the displacement $\mathbf{u}$, strain $\boldsymbol{\varepsilon}$, plastic strain $\boldsymbol{\varepsilon}^p$ and stress $\boldsymbol{\sigma}$, fields, such that:

$$\nabla \cdot \boldsymbol{\sigma} + \mathbf{f} = \mathbf{0} \tag{34a}$$

$$\boldsymbol{\sigma} = \mathbf{C} : (\boldsymbol{\varepsilon} - \boldsymbol{\varepsilon}^p) \tag{34b}$$

$$\boldsymbol{\varepsilon} = \nabla^s \mathbf{u} \tag{34c}$$

The field of plastic strains, $\boldsymbol{\varepsilon}^p$, is computed locally depending on the particular plastic model selected, but it can be considered as a certain function of the stress field and its history, $\boldsymbol{\varepsilon}^p = \boldsymbol{\varepsilon}^p(\boldsymbol{\sigma})$.

These equations, subjected to appropriate Dirichlet and Neumann boundary conditions, must be satisfied in Ω, the open and bounded domain of $\mathbb{R}^{n_{\text{dim}}}$ occupied by the solid in a space of n_{dim} dimensions.

4.1 The irreducible formulation

In the standard irreducible form of the elasto-plasticity problem Eq. (34c) is substituted into Eq. (34b), so that the stresses can be expressed in term of the displacement $\mathbf{u}$ and the plastic strain $\boldsymbol{\varepsilon}^p$ fields as:

$$\boldsymbol{\sigma} = \mathbf{C} : (\nabla^s \mathbf{u} - \boldsymbol{\varepsilon}^p) \tag{35}$$

The strong form of the irreducible problem reduces to Eq. (34a), once Eq. (35) is substituted, subjected to appropriate Dirichlet and Neumann boundary conditions. In the following, we will assume these in the form of prescribed displacements $\mathbf{u} = \overline{\mathbf{u}}$ on $\partial\Omega_u$, and prescribed tractions $\overline{\mathbf{t}}$ on $\partial\Omega_t$, respectively. The associated weak form is:

$$(\mathbf{v}, \nabla \cdot \boldsymbol{\sigma}) + (\mathbf{v}, \mathbf{f}) = 0 \qquad \forall \mathbf{v} \tag{36}$$

where $\mathbf{u},\ \mathbf{v} \in \mathcal{V}$ are the displacement field and its variations, $\mathcal{V} = H_0^1(\Omega)$ is the space of continuous functions with discontinuous derivatives, $L^2(\Omega)$ is the space of square integrable functions in Ω and $(\cdot, \cdot)$ denotes the inner product in $L^2(\Omega)$. Integrating Eq. (36) by parts, the problem can be rewritten in the standard form as:

$$(\nabla^s \mathbf{v}, \boldsymbol{\sigma}) - (\mathbf{v}, \mathbf{f}) - \left(\mathbf{v}, \overline{\mathbf{t}}\right)_{\partial\Omega} = 0 \qquad \forall \mathbf{v} \tag{37}$$

The *discrete* finite element form of the problem is obtained from Eq. (37) by substituting the displacement field and their variations by their standard finite element interpolations:

$$(\nabla^s \mathbf{v}_h, \boldsymbol{\sigma}_h) - (\mathbf{v}_h, \mathbf{f}) - \left(\mathbf{v}_h, \overline{\mathbf{t}}\right)_{\partial\Omega} = 0 \qquad \forall \mathbf{v}_h \tag{38}$$

where $\mathbf{u}_h, \mathbf{v}_h \in \mathcal{V}_h$ are the *discrete* displacement field and its variations, respectively.

4.2 The mixed $\mathbf{u}/p$ formulation

The strong form of the mixed $\mathbf{u}/p$ formulation for the J_2 plasticity continuum mechanical problem can be stated as: given the elastic properties (G, K) and prescribed body forces $\mathbf{f}$, find the displacement $\mathbf{u}$, pressure p, deviatoric strain $\mathbf{e}$, deviatoric plastic strain $\mathbf{e}^p$ and deviatoric stress $\mathbf{s}$, fields, such that:

$$\begin{aligned} \nabla \cdot \mathbf{s} + \nabla p + \mathbf{f} &= \mathbf{0} && (39a) \\ \nabla \cdot \mathbf{u} - \frac{1}{K} p &= 0 && (39b) \\ \mathbf{s} &= 2G\left(\mathbf{e} - \mathbf{e}^p\right) && (39c) \\ \mathbf{e} &= \operatorname{dev}\left(\nabla^s \mathbf{u}\right) && (39d) \end{aligned}$$

Note that in the mixed approach the pressure p is considered independent from the displament field.

Substituting Eq. (39d) into Eq. (39c) and this into Eq. (39a), the weak form of the problem (39a)-(39b) can be stated as:

$$\begin{aligned} (\mathbf{v}, \nabla \cdot \mathbf{s}) + (\mathbf{v}, \nabla p) + (\mathbf{v}, \mathbf{f}) &= 0 \qquad \forall \mathbf{v} && (40a) \\ (q, \nabla \cdot \mathbf{u}) - \left(q, \frac{1}{K} p\right) &= 0 \qquad \forall q && (40b) \end{aligned}$$

where $\mathbf{u},\ \mathbf{v} \in \mathcal{V} = H_0^1(\Omega)$ and $p\ ,\ q \in \mathcal{Q} = L^2(\Omega)$ are the displacement and pressure fields, respectively, and their variations. Integrating Eq. (40a) by parts, the problem can be rewritten in the standard form as:

$$\begin{aligned} (\nabla^s \mathbf{v}, \mathbf{s}) + (\nabla \cdot \mathbf{v},\, p) - (\mathbf{v}, \mathbf{f}) - \left(\mathbf{v}, \overline{\mathbf{t}}\right)_{\partial\Omega} &= 0 \qquad \forall \mathbf{v} && (41a) \\ (q, \nabla \cdot \mathbf{u}) - \left(q, \frac{1}{K} p\right) &= 0 \qquad \forall q && (41b) \end{aligned}$$

The *discrete* finite element form of the problem is obtained from Eqs. (41a)-(41b), substituting the displacement and pressure fields and their variations by their standard finite element interpolations:

$$\begin{aligned} (\nabla^s \mathbf{v}_h, \mathbf{s}_h) + (\nabla \cdot \mathbf{v}_h,\, p_h) - (\mathbf{v}_h, \mathbf{f}) - \left(\mathbf{v}_h, \overline{\mathbf{t}}\right)_{\partial\Omega} &= 0 \qquad \forall \mathbf{v}_h && (42a) \\ (q_h, \nabla \cdot \mathbf{u}_h) - \left(q_h, \frac{1}{K} p_h\right) &= 0 \qquad \forall q_h && (42b) \end{aligned}$$

where $\mathbf{u}_h\ ,\ \mathbf{v}_h \in \mathcal{V}_h$ and $p_h\ ,\ q_h \in \mathcal{Q}_h$ are the *discrete* displacement and pressure fields and their variations, defined onto the finite element spaces $\mathcal{V}_h$ and $\mathcal{Q}_h$, respectively.

4.3 The stabilized mixed $\mathbf{u}/p$ formulation

In mixed formulations, selection of the interpolating finite element spaces is not a trivial question. A major difficulty when using the standard Galerkin discrete form (42a)-(42b) is that the inf-sup condition (also known as Babuska-Brezzi or BB-condition) for stability poses severe restrictions on the choice of the spaces $\mathcal{V}_h$ and $\mathcal{Q}_h$ [22]. For instance, standard mixed elements with continuous equal order linear/linear interpolation for both fields are not stable, and the lack of stability shows as uncontrollable oscillations in the pressure field that usually, and very particularly in non linear problems, pollute the solution entirely.

Fortunately, the strictness of the BB-condition can be circumvented by modifying the discrete variational form appropriately, in order to attain the necessary global stability with the desired choice of interpolation spaces ([23], [24]). A particularly appealing consistent stabilization method is the *orthogonal sub-grid scale method (OSGS)*, originally developed for computational incompressible fluid mechanics problems ([25], [26]), and applied to the problem of incompressible elasto-plasticity, in small and finite strains, and continuum damage mechanics by the authors in previous works ([12], [13], [14], [15], [16] , [17], [18]).

The basic idea of the orthogonal sub-grid scale approach is to consider that the continuous displacement field can be split in two components, one coarse and a finer one, corresponding to different scales or levels of resolution. For the solution of the discrete problem to be stable it is necessary to, somehow, include the effect of both scales in the approximation. The coarse scale can be appropriately solved by a standard finite element interpolation, which however cannot solve the finer scale. Nevertheless, the effect of this finer scale can be included, at least locally, to enhance the stability of the pressure in the mixed formulation. It was argued in [26] that it is only natural to locate this unsolvable finer scale in the space orthogonal to the finite element space, referred to hereafter as $\mathcal{V}_h^\perp$. Therefore, the displacement field is approximated as

$$\mathbf{u} = \mathbf{u}_h + \widetilde{\mathbf{u}} \tag{43}$$

where $\mathbf{u}_h \in \mathcal{V}_h$ is the displacement component of the (coarse) finite element scale and $\widetilde{\mathbf{u}} \in \mathcal{V}_h^\perp$ is the enhancement of the displacement field corresponding to the (finer) sub-grid scale. Note that $\mathbf{u} \in \mathcal{V} \simeq \mathcal{V}_h \oplus \mathcal{V}_h^\perp$.

In order to ensure *consistency* of the stabilized mixed formulation, that is, that the stabilized discrete solution converges to the continuous solution

on mesh refinement , the sub-scale displacements are approximated in terms of the residual of Eq. (42a), $\mathbf{r}_h = \mathbf{r}_h(\mathbf{u}_h,\, p_h) = \nabla \cdot \mathbf{s}_h + \nabla p_h + \mathbf{f}$, as:

$$\widetilde{\mathbf{u}} = \tau_e\, P_h^{\perp}(\mathbf{r}_h) = \tau_e\, (\mathbf{r}_h - P_h(\mathbf{r}_h)) \quad \in \mathcal{V}_h^{\perp} \tag{44}$$

where P_h is the L_2–projection (least square fitting) onto $\mathcal{V}_h$ and $P_h^{\perp} = I - P_h$ is the corresponding orthogonal projection onto $\mathcal{V}_h^{\perp}$. The stabilization parameter $\tau_e = ch_e^2/2G_e^*$ is defined as a function of the characteristic length of the element h_e and the current secant shear modulus $2G_e^* = \|\mathbf{s}_h\| \,/\, \|\mathbf{e}_h\|$; c is a constant $c = \mathcal{O}(1)$.

Usually, the forces $\mathbf{f}$ can be assumed to belong to $\mathcal{V}_h$, so that $P_h^{\perp}(\mathbf{f}) = \mathbf{0}$. Also, $\nabla \cdot \mathbf{s}_h = 0$ when linear elements are used. In this case, expression (44) transforms in

$$\widetilde{\mathbf{u}} = \tau_e\ (\nabla p_h - P_h(\nabla p_h)) \tag{45}$$

Eq. (45) gives the value of the displacement subscale, which is added to the finite element displacement component as indicated in Eq. (43). This value of $\mathbf{u}$ is used in the weak form of the mixed formulation, Eqs. (41a)-(41b). The resulting *stabilized* mixed system of equations is :

$$(\nabla^s \mathbf{v}_h, \mathbf{s}_h) + (\nabla \cdot \mathbf{v}_h, p_h) - (\mathbf{v}_h, \mathbf{f}) - \left(\mathbf{v}_h, \overline{\mathbf{t}}\right)_{\partial\Omega_t} = 0 \qquad \forall \mathbf{v}_h \tag{46a}$$

$$(q_h, \nabla \cdot \mathbf{u}_h) - (\nabla q_h, \tau_e\, [\nabla p_h - \mathbf{\Pi}_h]) - \left(q_h, \frac{1}{K}\, p_h\right) = 0 \qquad \forall q_h \tag{46b}$$

When using linear/linear displacement and pressure interpolations, the only stabilization term appears in the incompressibility equation (46b), see [12], [13]. Observe that in the Eqs. (46a)-(46b) a third nodal variable $\mathbf{\Pi}_h$ appears, but this is not other that the L_2–projection of the pressure gradient, $\mathbf{\Pi}_h = P_h(\nabla p_h)$.

An alternative stabilization method is the one known as *Galerkin Least Square (GLS)*, originally proposed in [27]. The corresponding *stabilized discrete problem* reads:

$$(\nabla^s \mathbf{v}_h, \mathbf{s}_h) + (\nabla \cdot \mathbf{v}_h, p_h) - (\mathbf{v}_h, \mathbf{f}) - \left(\mathbf{v}_h, \overline{\mathbf{t}}\right)_{\partial\Omega_t} = 0 \qquad \forall \mathbf{v}_h \tag{47}$$

$$(q_h, \nabla \cdot \mathbf{u}_h) - (\nabla q_h, \tau_e \nabla p_h) - \left(q_h, \frac{1}{K}\, p_h\right) = 0 \qquad \forall q_h \tag{48}$$

which has a format very similar to the OSGS method, but does not require the computation of any extra nodal variable. Experience shows that the GLS method is more diffusive that the OSGS stabilization. This means that GLS is somewhat more "robust" than OSGS, but sometimes less sharp localizations are obtained.

5 Approximability of localized solutions in irreducible, mixed and enhanced formulations

In this Section we address the feasibility of modelling localized solutions using finite element formulations. In particular, we will consider the ability of irreducible and mixed formulations to reproduce in an adequate manner localization bands that aim to represent a regularized strong discontinuity and the necessity to enhance these formulations.

The very limited ability of standard finite elements to reproduce separation modes in general circumstances is well known [28]. Consider, for instance, a mesh of linear $P1$ constant strain triangles, such as the one in Figure 7, subjected to a separation motion in which the nodes located in the Ω^+ part of the domain have a relative displacement of $\mathbf{w}$ with respect the Ω^- part of the domain. Consider also, as in Figure 3a, that S^+ and S^- are two lines that run parallel to S (with normal $\mathbf{n}$), at a relative distance $b = h$, this being the typical height of the triangular elements. Surfaces S^+ and S^-delimit a localization band of width b inside which strain localization may occur. In this case, $\mathbf{w} = \mathbf{u}^+ - \mathbf{u}^-$ is the difference between the displacements at S^+ and S^- and $\boldsymbol{\beta} = \partial \mathbf{w} \,/\, \partial \xi$ is a deformation vector defined by differentiation with respect to the normal coordinate ξ.

With linear elements, the deformation vector $\boldsymbol{\beta}$ can only be approximated satisfactorily as $\boldsymbol{\beta} = \mathbf{w} \,/\, h$. This will, in fact, be the result obtained by projecting the exact separation mode on the finite element mesh of Figure 3a.

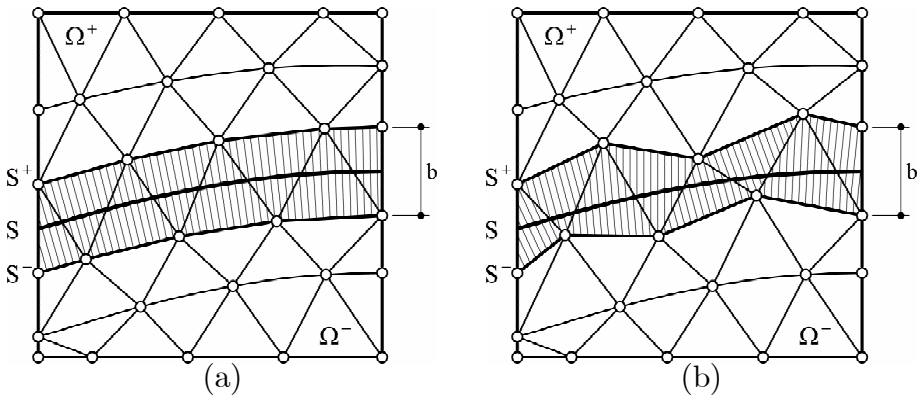

Figure 7: Finite element simulation of ocalized failure: (a) well-aligned and (b) mis-aligned meshes

However, projecting the exact separation mode onto the finite element mesh of Figure 3b, in which lines of nodes S^+ and S^- are not parallel to the intended discontinuity line, will not yield the same (correct) results. This is because $P1$ elements can only reproduce a constant deformation mode of the form required by Maxwell's compatibility condition $\boldsymbol{\varepsilon} = (\mathbf{n} \otimes \boldsymbol{\beta})^S$ if $\mathbf{n}$ is parallel to one of the sides of the triangles. The bilinear quadrilateral element $Q1$ shows similar shortcomings.

In particular, if we consider the problem of representing a slip separation mode, with $\mathbf{w}$ normal to $\mathbf{n}$, an incorrect representation of shear deformation results in volumetric locking. Mixed $P1P1$ or $Q1Q1$ elements display a slightly better behaviour than their corresponding irreducible counterparts, because incorporating an independent linear (or bilinear) interpolation of the pressure alleviates this fact. However, they share with the irreducible elements the same inherent problem with the deviatoric strain components.

The reason for this is that discrete solution spaces built from piecewise continuous polynomials cannot represent displacement discontinuities with arbitrary orientations inside the element, not even in a regularized fashion. This is purely an *approximability* shortage of the discrete solution spaces used, and does not show any disqualifying incapability of the formulation. However, the discomfiting approximability error is not eliminated nor reduced on mesh refinement.

The effective way of correcting this *approximability* local discretization error is to enrich the approximation spaces with additional deformation modes that enhance the desired capacities for representing embedded displacement and/or strain discontinuities. On one hand, the E-FEM ([29], [8], [30], [31], [32], [33], [34], [35], [36]) and the X-FEM ([37], [38], [39], [40], [41]) strategies aim to represent strong discontinuities as such, via elemental or nodal enhancements of the displacement solution space. On the other hand, in practice both formulations are often applied in a regularized manner ([42], [43], [44]), and in these regularized versions, the discrete solution considers embedded strain localization bands rather than actual displacement discontinuities. The width of the regularized band is regarded as a numerical parameter of the implementation, chosen to be "small". An obvious choice for this width is the size of the element, which, on mesh refinement, can be made as small as desired. This recovers the original idea of representing strong discontinuities in a smeared framework ([45], [46]).

Both irreducible and mixed finite element formulations can be enhanced with a suitable enrichment technique for the displacement and/or strain fields

to reduce the above discussed approximability error associated to the strain localization problem. In reference [47], the E-FEM approach is used together with a mixed displacement-pressure formulations to show improved approximation capabilities.

In any case, using an enhanced formulation, either with strain or displacement modes, requires to specify the orientation of the modelled discontinuity. This poses the question of when, along the deformation process, calculating and fixing this orientation. If the bifurcation, localization and decohesion conditions were fulfilled at the same time, that would be the instant to fix the discontinuity as a material surface; but this does not always happen. In general, a significant reorientation of the strain field may be needed until the plastic flow tensor has a structure compatible with the localization and decohesion conditions. Therefore, selecting the instant for the direction of the discontinuity according to some *ad hoc* condition and fixing it afterwards may be necessary in order to introduce the enhancing mode, but this must not become a superimposed condition on the constitutive behaviour.

6 Benchmark problems and numerical results

The numerical solution of the problem of bifurcation and localization discussed in the preceding sections is illustrated below in two selected benchmark problems. In both examples, strain localization is induced by the local J_2-plasticity model with exponential softening described in Section 2. Both plane stress and plane strain conditions are investigated. However, all computations are performed using a general 3D implementation, applied to a 3D solid domain with appropriate boundary conditions for each case considered. This ensures that the same implementation of the constitutive model is used for both plane stress and plane strain cases.

Relative performance of the irreducible displacement formulation and the stabilized mixed displacement/pressure formulation is tested considering meshes of *triangular* and *quadrilateral* prisms elements. The elements used will be: $Q1Q1$ (bilinear displacement/bilinear pressure, $Q1$ (bilinear displacement), $P1P1$ (linear displacement/ linear pressure, $P1$ (linear displacement). Only low order elements are considered because they are more effective in problems involving sharp displacement and strain gradients. When the stabilized mixed displacement/pressure formulation is used, a value $c = 0.1$ is taken for the evaluation of the stabilization parameter τ_e.

The following material properties are assumed: Young's modulus $E = 10$ MPa, Poisson's ratio $\nu = 0.3$ (recall that $G = E/2\,(1+\nu)$, $K = E/3\,(1-2\nu)$), uniaxial yield stress $\sigma_o = E/1000 = 10$ KPa and fracture energy $\mathcal{G} = 300$ J/m^2.

The geometry considered for the benchmark problems is depicted in Figure 8. It consists of a square plate subjected to an imposed field of uniform horizontal ($\sigma_x = \sigma_1$) and vertical ($\sigma_y = \sigma_2$) normal stresses applied at the lateral boundaries. In-plane dimensions of the plate are 20×20 m $\times$ m and its thickness is 0.125 m. In order to induce bifurcation and localization of the solution in a controlled fashion, a small imperfection is introduced in the form of a square opening of 0.25×0.25 m $\times$ m in the center of the plate. Because of the double symmetry, only one quarter of the domain (the top right quarter) needs to be considered, with appropriate symmetry boundary conditions at the left and bottom boundaries.

In all of the analyses performed the square domain is discretized into a regular grid of $h = 0.125$ m. The width of the localization band required for the softening regularization procedure described in Section 2 has been

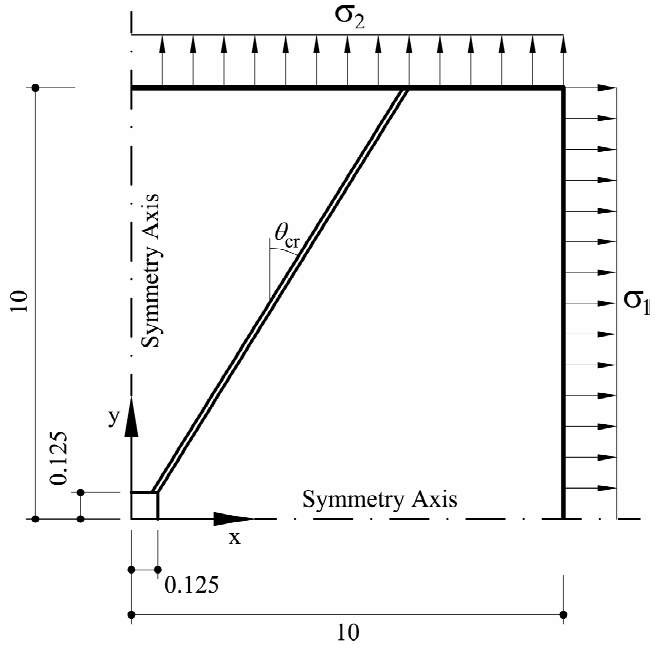

Figure 8: Geometry and dimensions for benchmark problems

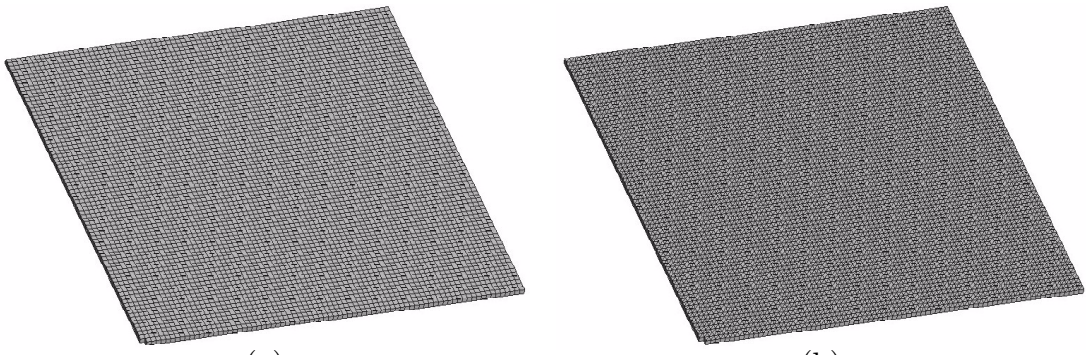

(a) (b)

Figure 9: (a) $Q1Q1$ and (b) $P1P1$ FE meshes used for benchmark problem

taken equal to this grid resolution $b = h = 0.125$ m. The resulting 3D meshes are shown in Figures 9a and b, composed of a uniform 80×80 mesh of quadrilateral prisms and a uniform $80 \times 80 \times 2$ mesh of rectangular triangular prisms, respectively. Notice that both meshes are structured: all of the element sides in the quadrilateral mesh are at 0^o or 90^o with the horizontal axis, all of the element sides in the triangular mesh are at 0^o, 45^o or 90^o with the horizontal axis.

The discrete problem is solved incrementally, in a (pseudo)time step-by-step manner. Analyses are performed under displacement control in order to trace the complete post-peak behavior. An automatic time incrementation procedure is used to reduce the size of the time steps when convergence due to the nonlinear effects is more difficult. About 200 steps are necessary to complete the analyses. Within each step, a modified Newton-Raphson method, together with a line search procedure, is used to solve the corresponding non-linear system of equations. Convergence of a time step is attained when the ratio between the norm of the iterative and the incremental norm of the residual arrays is lower than 10^{-3}. It has to be remarked that no tracking algorithm of any sort has been used in any of the computations. Likewise, the analytical results obtained in Section 3 are not used in any way in the numerical computations; they are only referred to in this Section for benchmarking purposes.

Calculations are performed with an enhanced version of the finite element program COMET [48], developed at the International Center for Numerical Methods in Engineering (CIMNE). Pre and post-processing is done with GiD, also developed at CIMNE [49].

6.1 Plane stress conditions

In the first place, bifurcation and localization under plane stress conditions are investigated. To this end, displacements in the direction transversal to the plate are left free, save for one which is fixed in order to avoid rigid body motions.

6.1.1 Quadrilateral prisms elements

Firstly, the performance of mixed $Q1Q1$ and irreducible $Q1$ quadrilateral prisms is examined. Figures 10 and 11 report results for the mixed and the standard elements, respectively. In both figures, the four different rows correspond to the four different stress combinations investigated, which are the same ones depicted in Figure 5 and the corresponding Table 2 , namely: (a) **P1**: $\sigma_1/\sigma_2 = 1.0$ /-1.0, $\theta = 45°$, (b) **P2**: $\sigma_1/\sigma_2 = 1.0$ / 0.0, $\theta = 35.26°$, (c) **P3**: $\sigma_1/\sigma_2 = 1.0$ / 0.25, $\theta = 28.12°$, (d) **P4**: $\sigma_1/\sigma_2 = 1.0$ / 0.50, $\theta = 0°$. The right hand side column in both Figures shows contours for horizontal displacements once the localization band in fully developed, while the right hand side column displays corresponding contours for the equivalent plastic strain.

It is clear in Figure 10, that the mixed quadrilateral elements are capable of solving the bifurcation and localization problem under plane stress conditions rather satisfactorily. For load case **P1**, pure shear, an exact angle of $\theta = 45°$ is obtained, and the simulated slip line bifurcates near the top right corner because of the perfectly symmetric boundary conditions. For load cases **P2** and **P3**, the obtained direction for the localization differ from the analytical values in less that 1°. Only a slight deviation from this occurs in the vicinity of the central opening; this can be partly attributed to the effect of the disturbed field and partly to a minor mesh bias. For load case **P4**, the localization direction is again exact.

It is remarkable that with the same constitutive behaviour, namely a purely isochoric plastic model, it is possible to obtain from a pure mode II response (relative displacement across the localization band $\mathbf{w}$ orthogonal to the normal to the band $\mathbf{n}$), like in the **P1** case, to a pure mode I response (relative displacement across the localization band $\mathbf{w}$ parallel to the normal to the band $\mathbf{n}$), like in the **P4** case; and, naturally, mixed mode responses in between.

Note the resolution of the discontinuity surfaces achieved by the finite

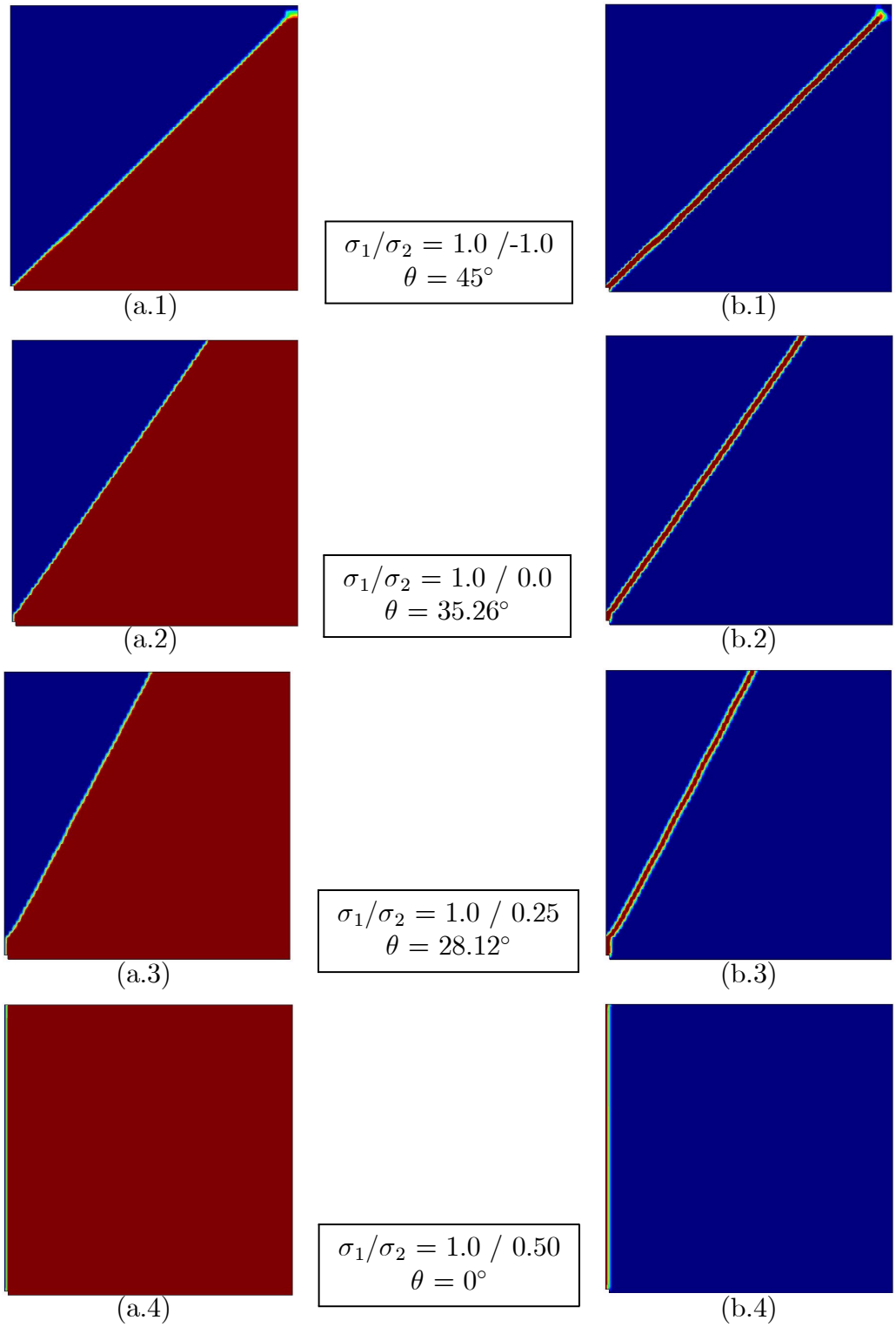

Figure 10: Results for **plane stress** conditions with *Q1Q1* mixed quadrilateral prism elements. Contours for: (a) horizontal displacement and (b) equivalent plastic strain

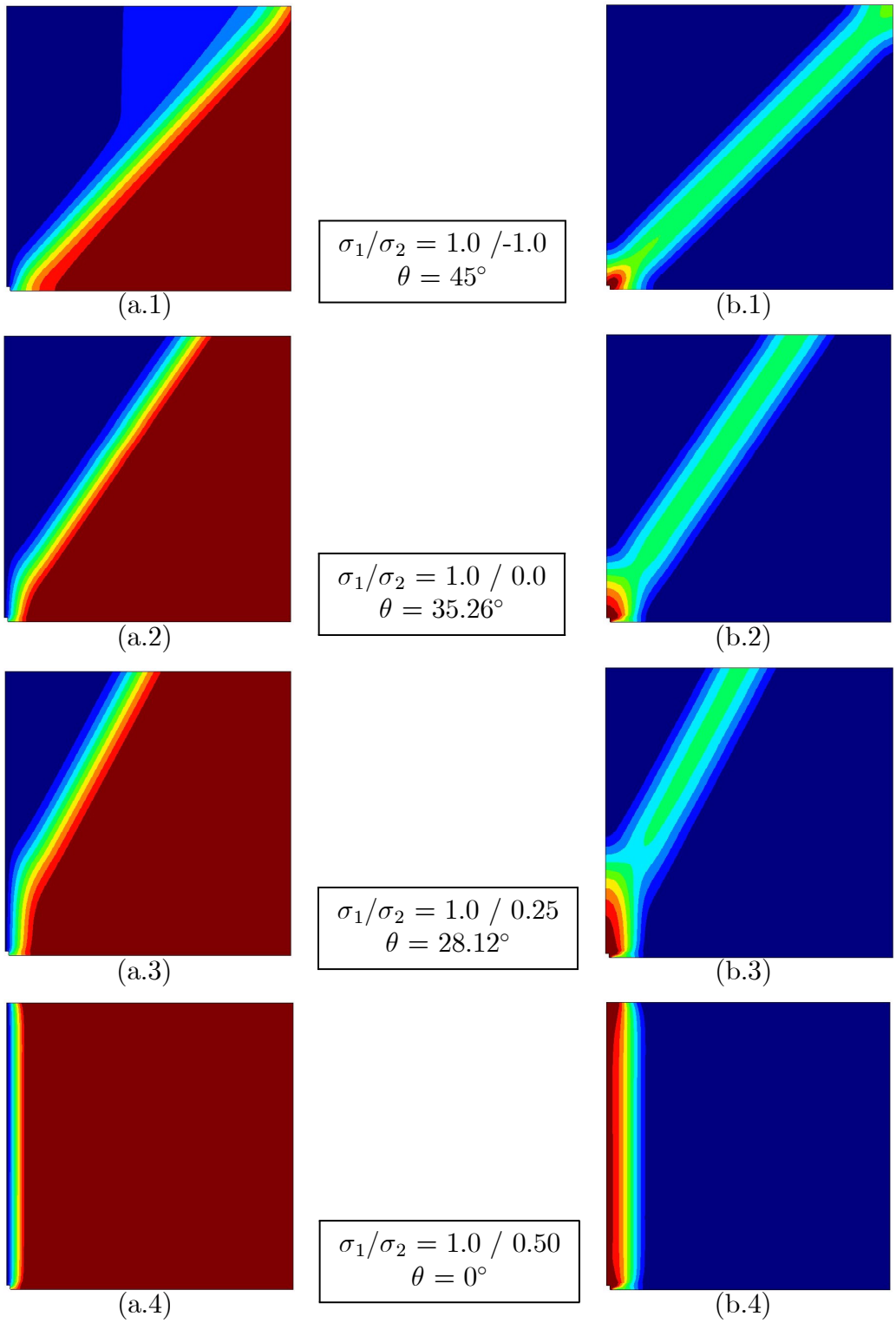

Figure 11: Results for **plane stress** conditions with *Q1* irreducible quadrilateral prism elements. Contours for: (a) horizontal displacement and (b) equivalent plastic strain

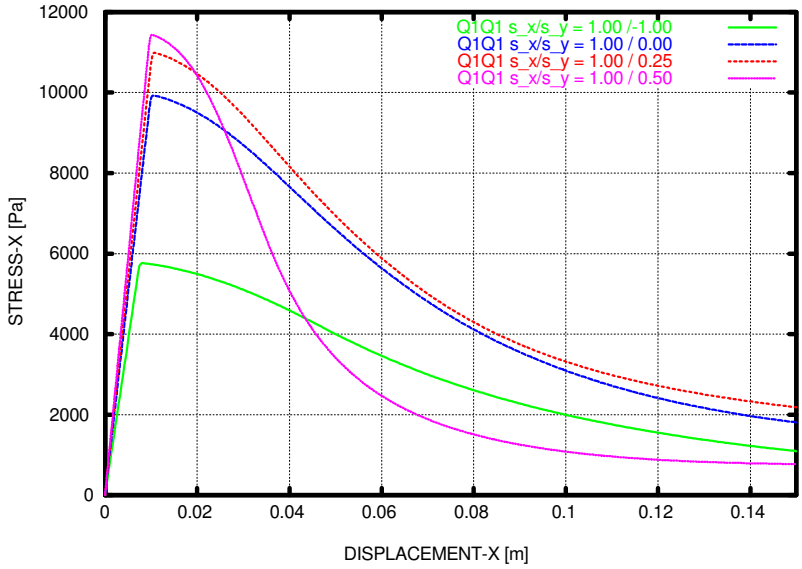

(a) $Q1Q1$ mixed elements

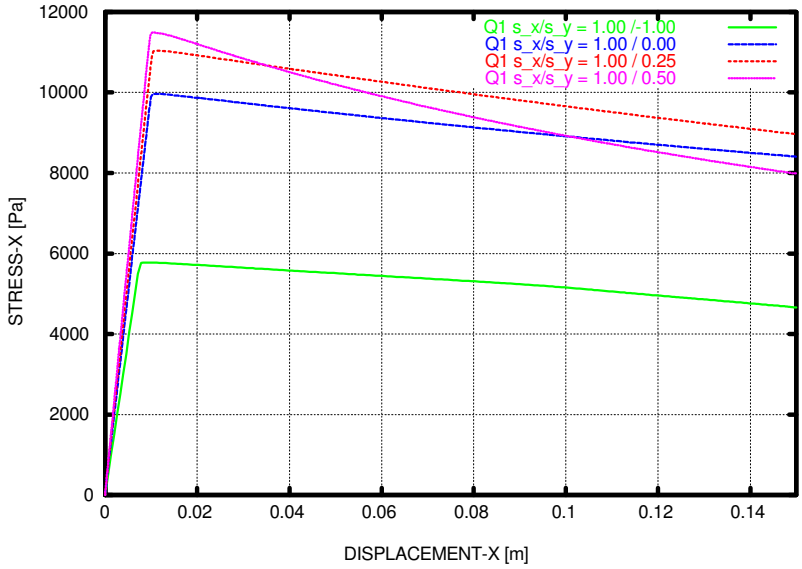

(b) $Q1$ irreducible elements

Figure 12: Horizontal stress *versus* horizontal displacement for **plane stress** conditions with mixed and irreducible quadrilateral prism elements

element solution is optimal for the displacement and strain interpolations used: the strong discontinuity is regularized into a band which is only one element across.

Figure 11 shows results obtained with the irreducible quadrilateral prisms $Q1$. The standard formulation is able to solve correctly the bifurcation and discontinuous bifurcation conditions, but clearly unable to comply with the decohesion condition. For the four depicted situations strain localization bands form at the angles predicted by the analytical results in Section 3. This is not surprising because, in this benchmark setting, the far field stress state is exactly provided by the applied boundary conditions. However, the volumetric locking that accompanies (plastic) strain localization makes it impossible for the band to collapse into a regularized strong discontinuity that approaches the decohesive limit asymptotically.

Figures 12a and 12b render plots of applied σ_x versus horizontal displacement at the right bottom point of the studies quarter plate for the mixed and irreducible quadrilateral elements, respectively. As commented in Section 3.1.1, under plane stress situations, the onset of yielding, bifurcation and localization occur at the same instant. Also, from the same moment at which plastic flow is initiated this manifests in a direction that is compatible with the decohesion condition. On one hand, these facts are clear in the top Figure, which shows curves corresponding to well developed failure mechanisms. The limit cases: **P1** for mode II and **P4** for mode I are particularly interesting. On the other hand, the bottom Figure 12b clearly shows the locking volumetric effect inherent to irreducible low order elements in quasi-incompressible situations. The bifurcation and localization points are reached correctly, because they depend only on the elastic regime, and this is well resolved by the mesh. However, volumetric locking induced by the isochoric character of the plastic flow distorts the strain field in such a manner than the decohesion condition cannot be fulfilled.

6.1.2 Triangular prisms elements

Secondly, the performance of mixed $P1P1$ and irreducible $P1$ triangular prisms is examined. Figures 13 and 14 report results for the mixed and the standard elements, respectively. The same stress combinations as in the previous Section are investigated.

Figure 13 shows that the mixed triangular elements solve the bifurcation and localization problem under plane stress conditions in the same adequate

manner than their quadrilateral counterparts. Their respective results are indistinguishable. On its part, Figure 14 shows that the irreducible triangular elements have similar shortcoming as their quadrilateral companions. However, some differences may be found between Figures 11 and 14. For the pure shear case, $\sigma_1/\sigma_2 = 1.0$ /-1.0, the irreducible triangles do manage to yield the correct solution. This befalls because the used finite element mesh happens to be perfectly aligned with the correct localization direction. For uniaxial tension, $\sigma_1/\sigma_2 = 1.0$ / 0.0, another interesting feature can be observed, the mesh initiates smeared localization in the correct direction, but eventually mesh-bias takes over and a sharp localization happens, but at the wrong direction. For the other two cases, results are indistinguishable from those of the quadrilaterals, strongly affected by volumetric strain locking.

Figures 15a and 15b portray plots of applied σ_x versus horizontal displacement at the right bottom point of the studies quarter plate for the mixed and irreducible quadrilateral elements, respectively. They can be easily interpreted with regard to those corresponding to quadrilateral elements and the already mentioned differences. The fact that the softening branches in Figures 12a and 15a are not identical reflects that we have used an identical localization width $b = h$, equal to the grid step, for all cases. A more precise definition of the localization width, depending on the actual projection of the considered element on the direction of strain localization, would render better correspondence between the different elements [20].

6.2 Plane strain conditions

In the second place, bifurcation and localization under plane strain conditions are investigated. To this end, displacements in the direction transversal to the plate are all fixed equal to zero; this ensures that normal strain in that direction is exactly equal to zero.

6.2.1 Quadrilateral prisms elements

The performance of mixed $Q1Q1$ and irreducible $Q1$ quadrilateral prisms is examined first. Figures 16 and 17 report results for the mixed and the standard elements, respectively. In both figures, the four different rows correspond to the four different stress combinations investigated, which are the same ones depicted in Figure 6 and the corresponding Table 3 , namely: (a) **P1**: $\sigma_1/\sigma_2 = 1.0$ /-1.0, (b) **P2**: $\sigma_1/\sigma_2 = 1.0$ / 0.0, (c) **P3**: $\sigma_1/\sigma_2 = 1.0$ / 0.25,

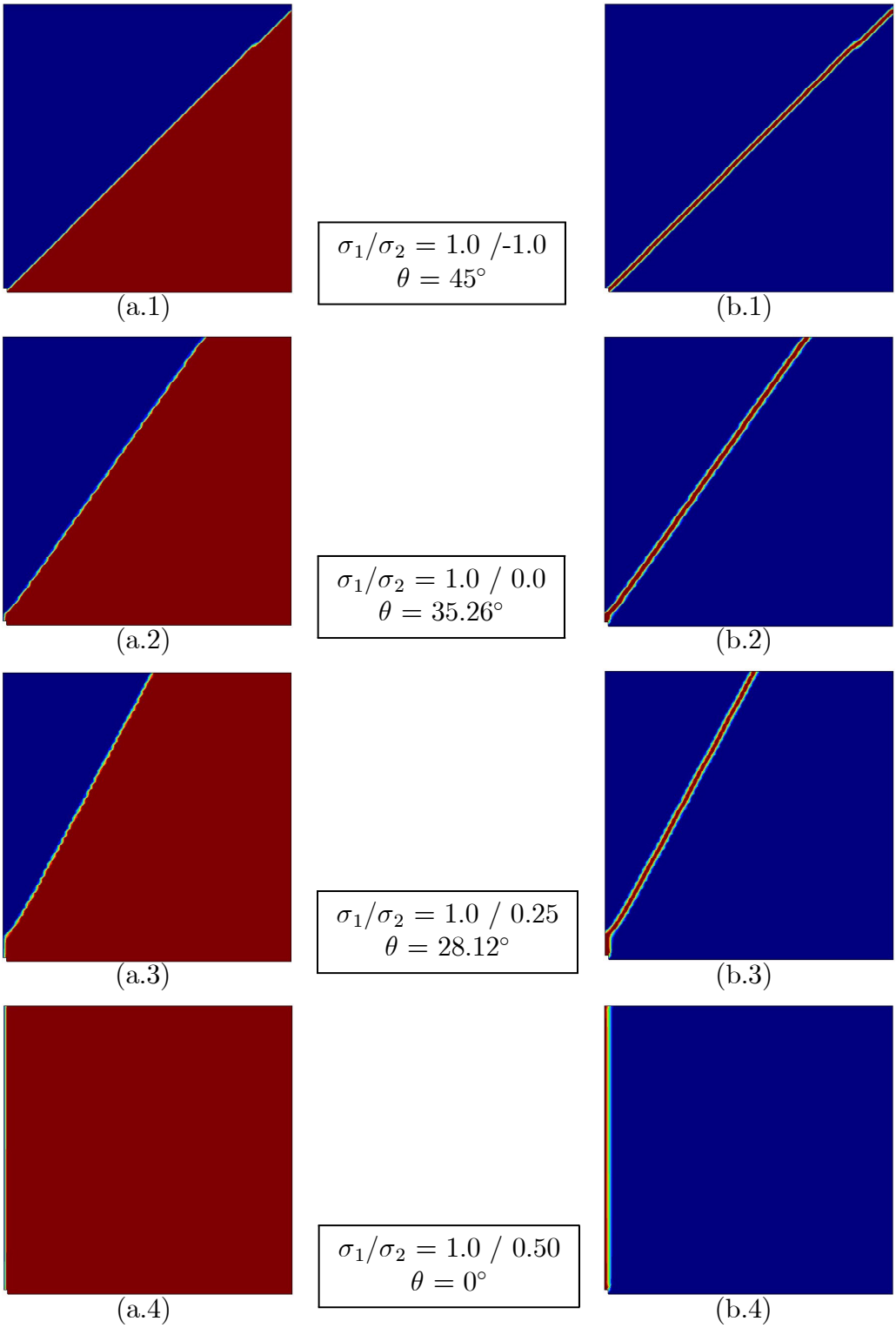

Figure 13: Results for **plane stress** conditions with *P1P1* mixed triangular prism elements. Contours for: (a) horizontal displacement and (b) equivalent plastic strain

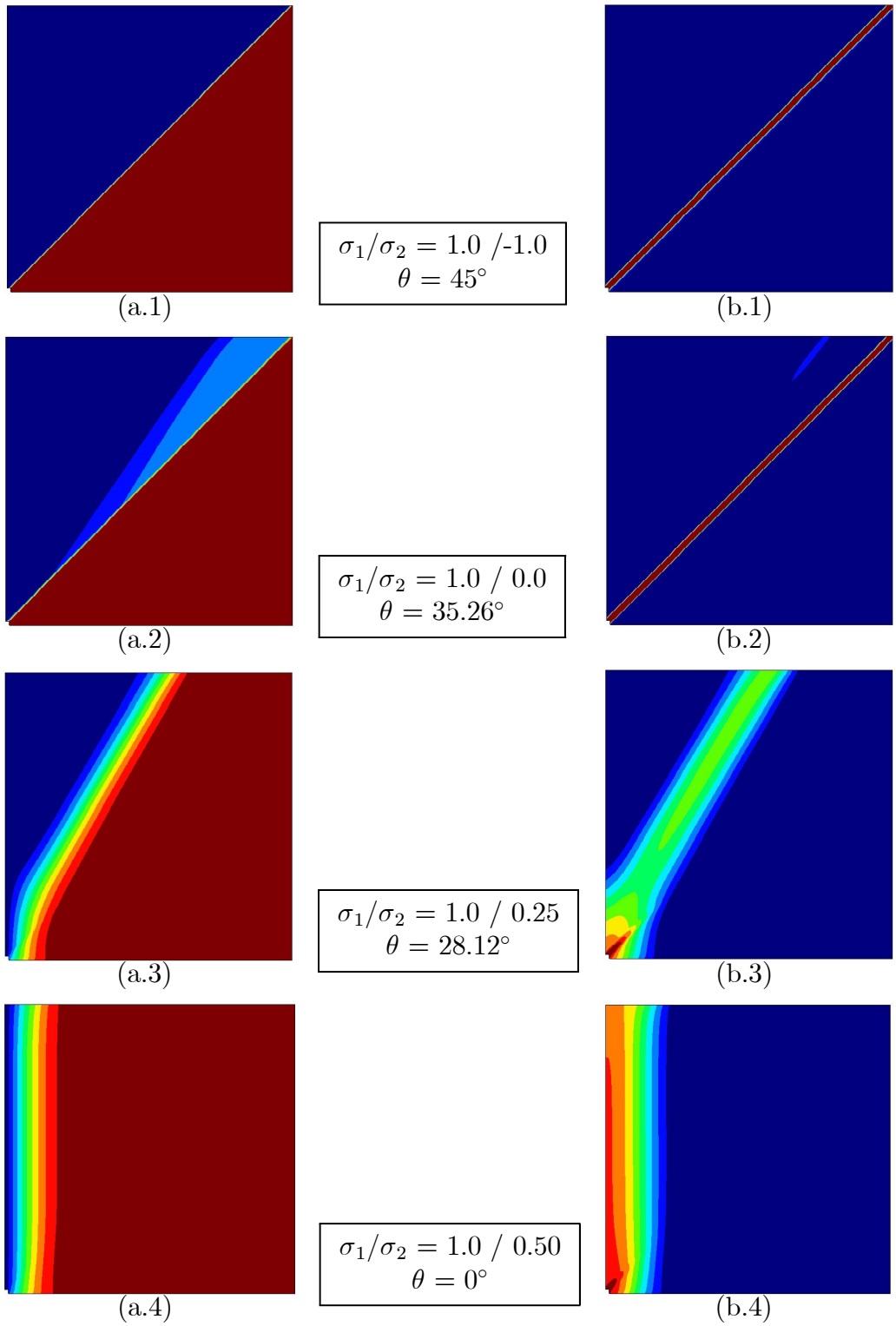

Figure 14: Results for **plane stress** conditions with *P1* irreducible triangular prism elements. Contours for: (a) horizontal displacement and (b) equivalent plastic strain

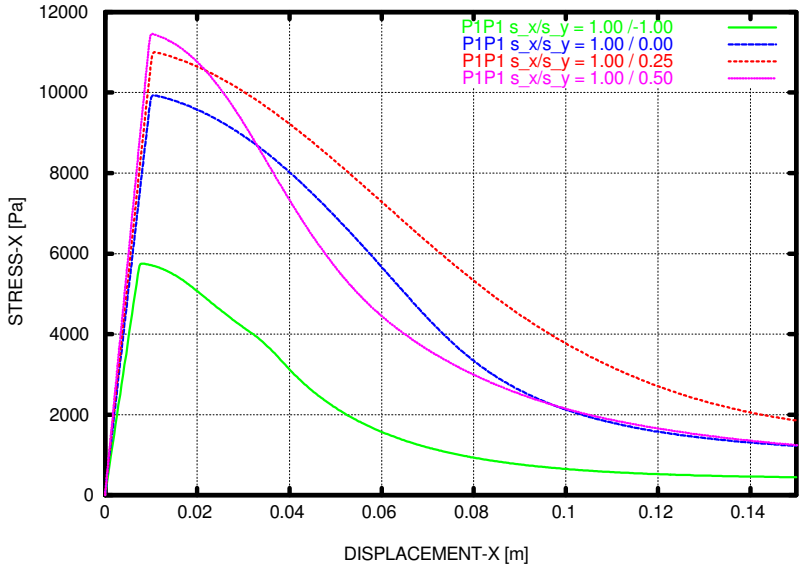

(a) $P1P1$ mixed elements

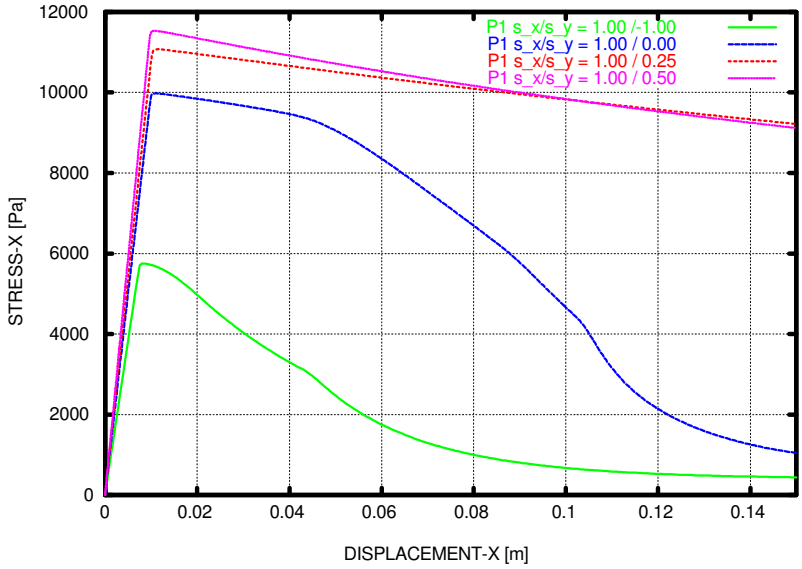

(b) $P1$ irreducible elements

Figure 15: Horizontal stress *versus* horizontal displacement for **plane stress** conditions with mixed and irreducible triangular prism elements

(d) **P4**: $\sigma_1/\sigma_2 = 1.0$ / 0.50. In all cases, the localization angle is identical, $\theta = 45^\circ$. The right hand side column in both Figures shows contours for horizontal displacements once the localization band in fully developed, while the right hand side column displays corresponding contours for the equivalent plastic strain.

Figures 16 and 17 show that the bifurcation and localization problem is more demanding on finite elements under plane strain conditions than in a plane stress situation. This is because for the decohesion condition to be met and a regularized strong discontinuity to develop, a significant amount of strain reorientation has to occur through the growth of plastic flow.

Figure 16 proves that the mixed quadrilateral elements are capable of reproducing the necessary reorientation of the strain flow in all but the most difficult case, **P4.** In the first three cases, the (regularized) strong discontinuity is correctly formed, but in the last fourth case, the mesh is too rigid to allow for the collapse of the localization band, which forms at the correct direction, into a discontinuity with no traction cohesion. The situation is far worse in Figure 17, which shows that the irreducible quadrilateral elements cannot properly localize strains in any of the tested cases. In the last case, not even a smeared localization band is visible in the displacement and plastic strain contour plots.

Figures 18a and 18b are consistent with these explanations.

6.2.2 Triangular prisms elements

Finally, the performance of mixed $P1P1$ and irreducible $P1$ triangular prisms is examined. Figures 19 and 20 report the corresponding results.

Figure 19 shows that the mixed triangular elements solve the demanding bifurcation and localization problem under plane strain conditions slightly better than their quadrilateral counterparts. Comparing these with results in 19, it is immediately perceived that triangular elements solve satisfactorily all the cases considered. This is because the triangular mesh is more flexible than the quadrilateral one, and particularly for the deformation mode called for in these tests. Figure 20 depicts an impeccable performance by the irreducible triangular elements for this problem. This is because the used finite element mesh happens to be perfectly aligned with the correct localization direction.

Figures 21a and 21b present plots of applied σ_x versus horizontal displacement at the right bottom point of the studies quarter plate for the mixed and irreducible triangular elements, respectively. The top and bot-

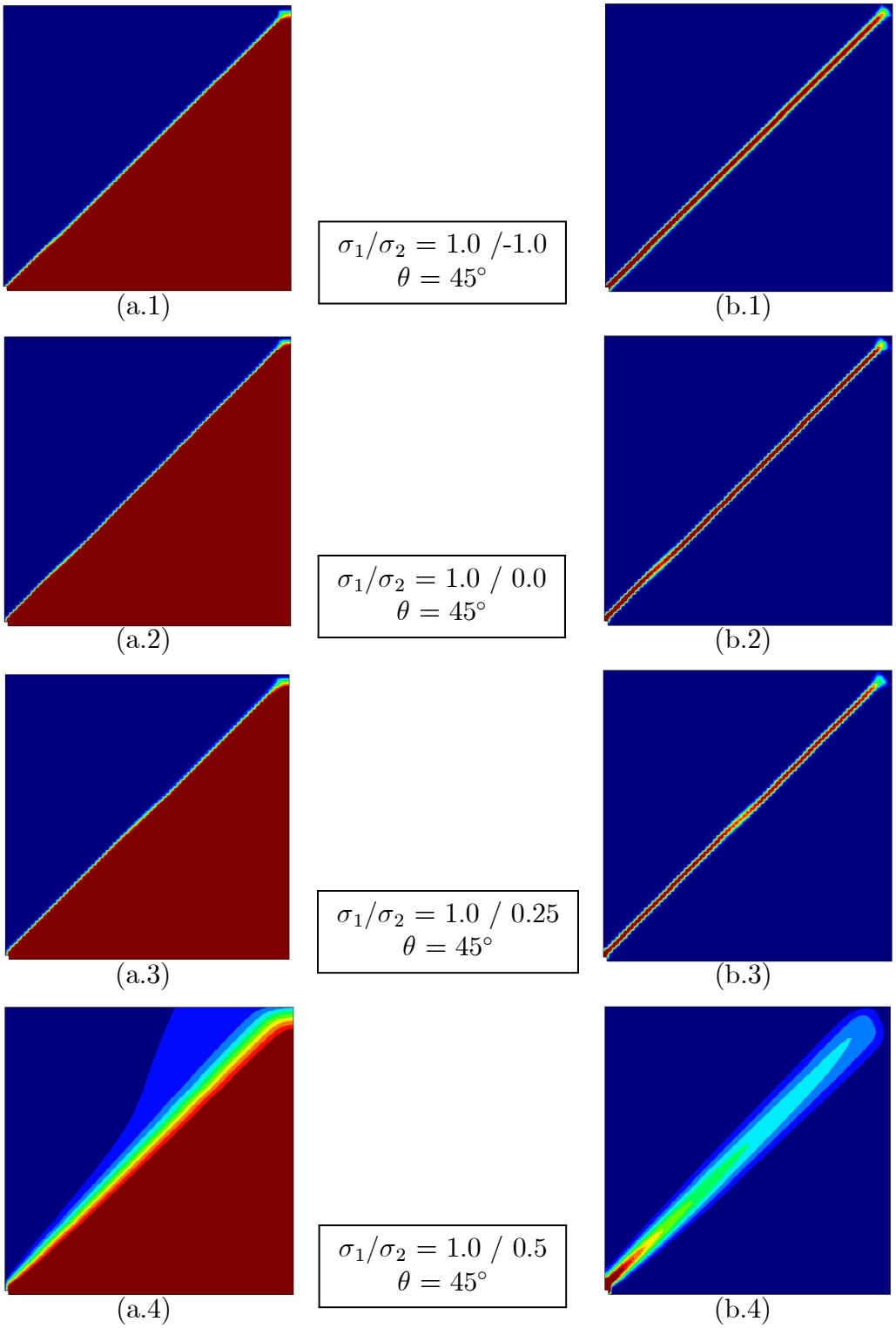

Figure 16: Results for **plane strain** conditions with *Q1Q1* mixed quadrilateral prism elements. Contours for: (a) horizontal displacement and (b) equivalent plastic strain

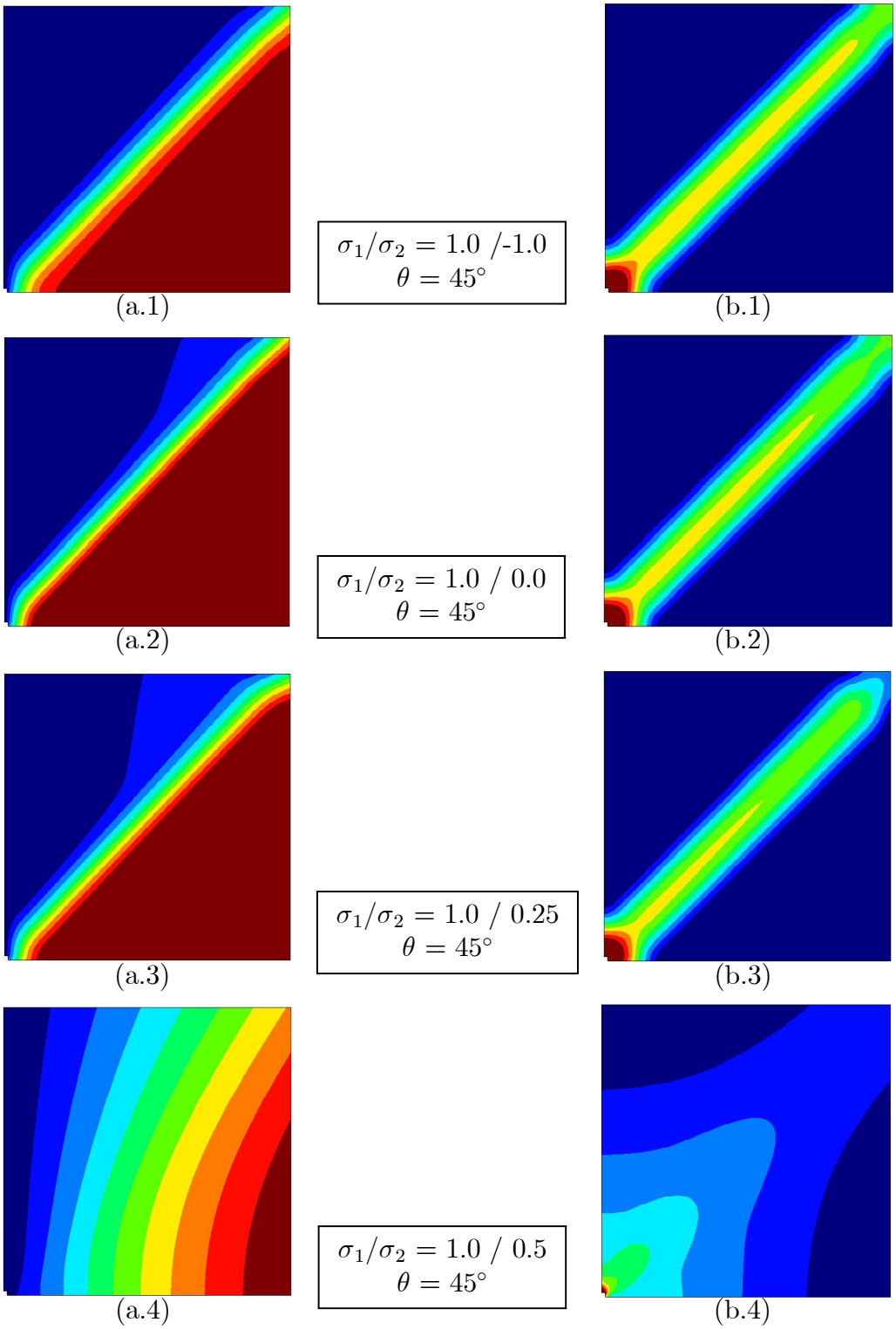

Figure 17: Results for **plane strain** conditions with *Q1* irreducible quadrilateral prism elements. Contours for: (a) horizontal displacement and (b) equivalent plastic strain

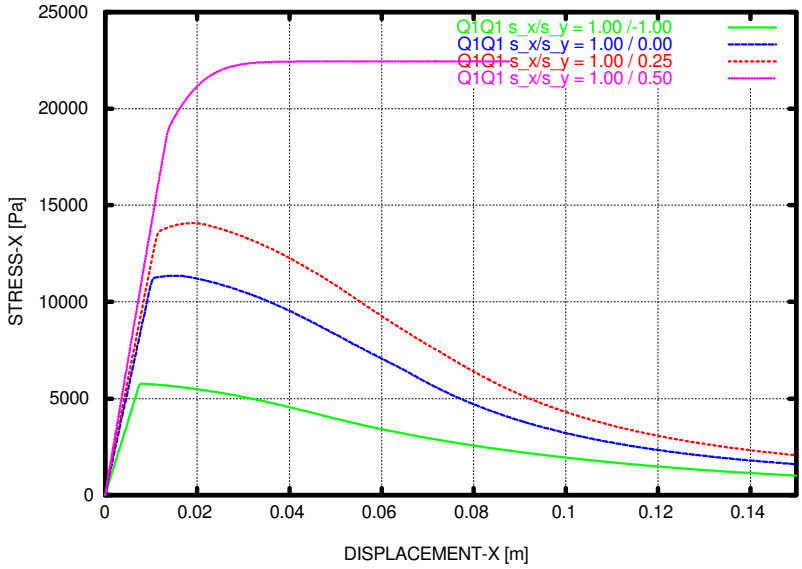

(a) $Q1Q1$ mixed elements

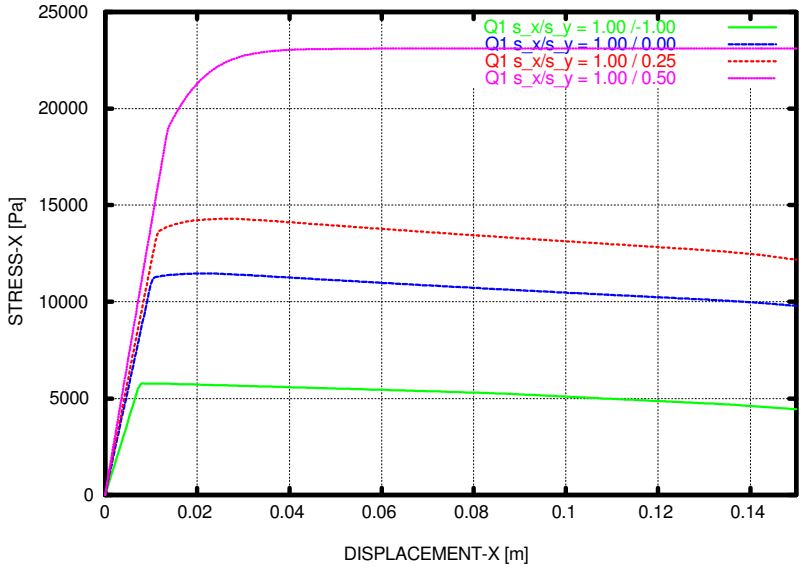

(b) $Q1$ irreducible elements

Figure 18: Horizontal stress *versus* horizontal displacement for **plane strain** conditions with mixed and irreducible quadrilateral prism elements

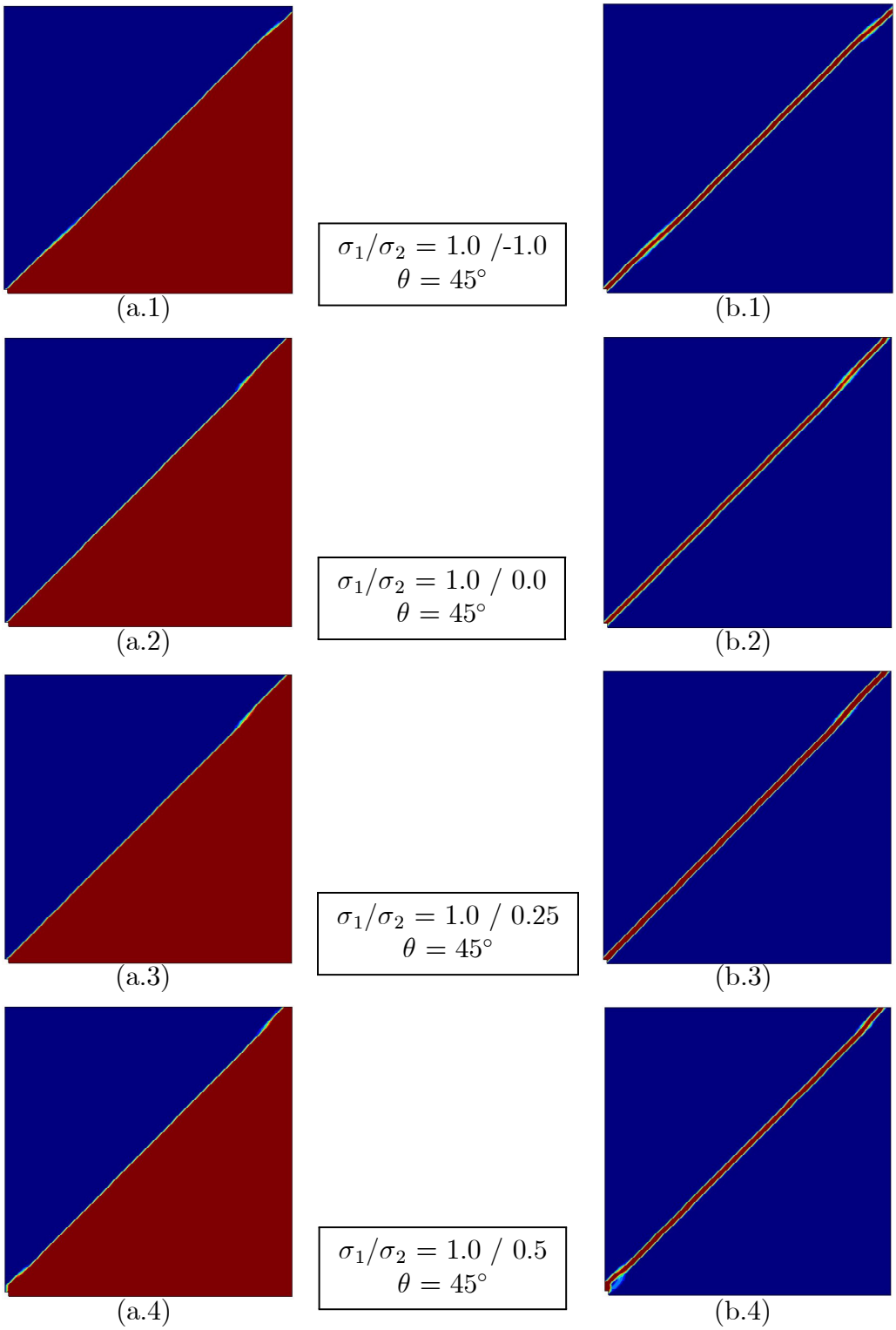

Figure 19: Results for **plane strain** conditions with *P1P1* with mixed triangular prism elements. Contours for: (a) horizontal displacement and (b) equivalent plastic strain

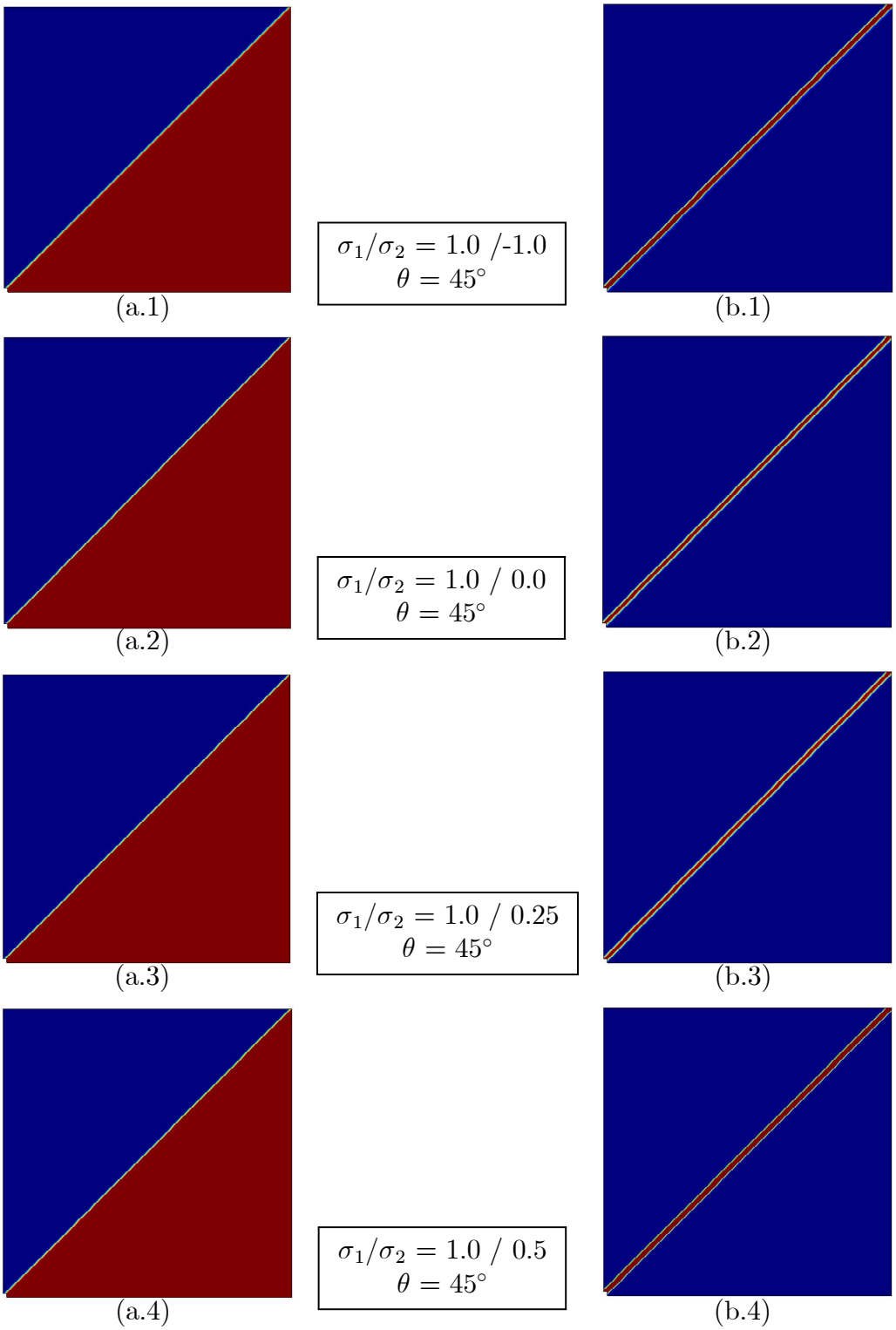

Figure 20: Results for **plane strain** conditions with *P1* with irreducible triangular prism elements. Contours for: (a) horizontal displacement and (b) equivalent plastic strain

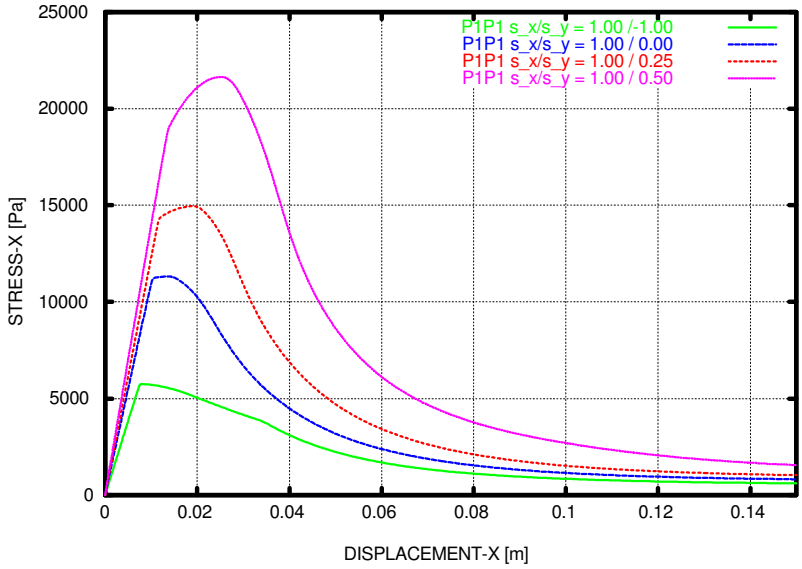

(a) $P1P1$ mixed elements

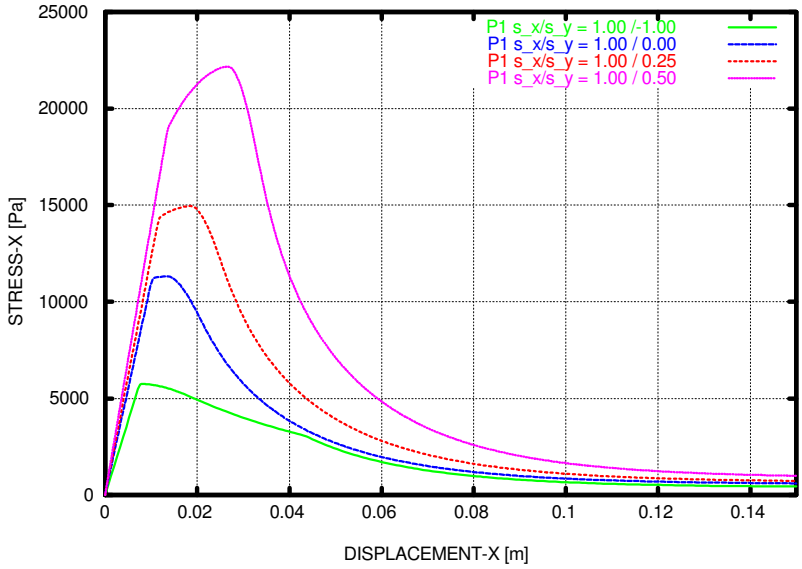

(b) $P1$ irreducible elements

Figure 21: Horizontal stress *versus* horizontal displacement for **plane strain** conditions mixed and irreducible triangular prism elements

tom graphs are remarkably similar. This is not surprising as the predicted failure mechanisms are correctly computed in all cases. It is observed that the computed dissipated energy is marginally larger in the mixed case; this may be attributed to the very minor variations observable between Figures 19 and 20. Differences between these results and those in Figures 18a reflect again that we have used an identical localization width $b = h$, equal to the grid step, for all cases.

7 Conclusions

This paper considers the problem of strain bifurcation and localization in J_2 plasticity under plane stress and plane strain conditions.

First, distinction is made among the analytical necessary bifurcation, localization and decohesion conditions. On one hand, this shows that results from classical localization analysis do not in general guarantee that the decohesion limit may be reached; on the other hand, localization angles can be obtained by directly imposing this condition.

Second, the mixed (displacement/pressure) formulation are considered for the solution of the associated discrete problem, characterized by the isochoric nature of the purely deviatoric plastic flow. Stabilization is necessary for the case or using equal order interpolating spaces for displacements and pressure. Even if not specifically designed for this purpose, the mixed formulation reduces the approximability error that low order elements display when reproducing (regularized) discontinuous displacement fields, if the direction of the discontinuity is not parallel to one of the element sides.

Numerical examples demonstrate the relative performance of the mixed and irreducible quadrilateral and triangular (prisms) elements subjected to plane stress and plane strain conditions. It can be concluded that the mixed displacement/pressure formulation shows a tremendous superiority over the irreducible one to predict correct failure mechanisms with localized patterns of plastic deformation, which are practically free from dependence of the mesh directional bias in all but the most demanding cases. Irreducible elements suffer strongly from volumetric strain locking as soon as plastic behaviour appears and this precludes strain localization to reach its ultimate consequences and therefore, localization bands fails to collapse in true failure mechanisms. In the limited cases in which the failure mechanism actually forms, it is very much affected by the mesh bias. Only when the mesh is well aligned with

the correct failure mechanism satisfactory results are obtained.

8 Acknowledgments

Financial support from the Spanish Ministry for Education and Science under the *SEDUREC* project (CSD2006-00060) is also acknowledged.

References

[1] Hill, R. 1958. General theory of uniqueness and stability of elasto-plastic solids, J. Mech. Phys. Solids, 6, 236-249.

[2] Ottosen, N. and Runesson, K., 1991. Properties of discontinuous bifurcation solutions in elasto-plasticity. Int. J. Solids and Structures 27(4), 401-421.

[3] Runesson, K., Ottosen, N.S., and Peric, D., 1991. Discontinuous bifurcations of elastic-plastic solutions at phase stress and plane strain. Int. J. of Plasticity 7, 99-121.

[4] Steinmann, P. and Willam, K., 1994. Finite element analysis of elastoplastic discontinuities. Journal of Engineering Mechanics 120, 2428-2442.

[5] Iordache, M. M., 1996. Failure analysis of classical and micropolar elastoplastic materials. report CU/SR-96/2. Department of Civil, Enviromental and Archetectural Engineering, University of Colorado.

[6] Iordache, M.M. and Willam, K. 1998. Localized failure analysis in elastoplastic Cosserat continua. Comp. Meth. Appl. Mech. Engrg. 151, 559-586.

[7] Manzoli, O., Oliver, J. and Cervera, M., 1998. Localización de deformaciones: análisis y simulación numérica de discontinuidades en mecánica de sólidos (in Spanish). Monograph 44, CIMNE, Barcelona, Spain.

[8] Oliver, J., Cervera, M. and Manzoli, O. 1999. Strong discontinuities and continuum plasticity models: the strong discontinuity approach. Int. J. of Plasticity, 15, 319-351.

[9] Willam, K., 2000. Constitutive Models for Materials. Encyclopedia of Physical Science Technology. 3rd Edition. Academic Press.

[10] Willam, K. and Iordache, M. M., 2001. On the lack of simmetry in materials. Trends in computational structural mechanics. In: W.A. Wall, K.U. Bletzinger and K. Schweizerhof (Eds.) CIMNE, Barcelona, Spain.

[11] Simo, J.C. and Hughes, T.J.R. 1998. Computacional Inelasticity. Interdisciplinary Applied Mathematics. Vol. 7. Springer.

[12] Chiumenti, M., Valverde, Q., Agelet de Saracibar, C. and Cervera, M., 2002. A stabilized formulation for incompressible elasticity using linear displacement and pressure interpolations, Comp. Meth. in Appl. Mech. and Eng., 191, 5253-5264.

[13] Cervera, M., Chiumenti, M., Valverde, Q. and Agelet de Saracibar, C. 2003. Mixed Linear/linear Simplicial Elements for Incompressible Elasticity and Plasticity. Comp. Meth. in Appl. Mech. and Eng., 192, 5249-5263.

[14] Cervera, M., Chiumenti, M. and Agelet de Saracibar, C. 2003. Softening, localization and stabilization: capture of discontinuous solutions in J2 plasticity. Int. J. for Num. and Anal. Meth. in Geomechanics, 28, 373-393.

[15] Cervera, M., Chiumenti, M. and Agelet de Saracibar, C. 2003. Shear band localization via local J_2 continuum damage mechanics. Comp. Meth. in Appl. Mech. and Eng., 193, 849-880.

[16] Chiumenti, M., Valverde, Q., Agelet de Saracibar, C. and Cervera, M., 2004. A stabilized formulation for incompressible plasticity using linear triangles and tetrahedra, Int. J. of Plasticity, 20, 1487-1504.

[17] Agelet de Saracibar, C., Chiumenti, M., Valverde, Q. and Cervera, M., 2006. On the orthogonal subgrid scale pressure stabilization of finite deformation J_2 plasticity. Comp. Meth. in Appl. Mech. and Eng., 195, 1224-1251.

[18] Cervera, M. and Chiumenti, M. Size effect and localization in J_2 plasticity, Int. J. of Solids and Structures (2009) 46, 3301-3312.

[19] Bazant, Z.P. and Oh, B.H. 1983. Crack band theory for fracture of concrete. Materials and Structures, 16, 155-177.

[20] Oliver, J., 1989. A consistent characteristic length for smeared cracking models. Int. J. Num. Meth. Engng., 28, 461-474.

[21] Oliver, J., Huespe, A.E. Pulido, M.D.G. and Chaves, W.V. 2002. From continuum mechanics to fracture mechanics: the strong discontinuity approach. Engineering Fracture Mechanics, 69, 113-136.

[22] Brezzi, F. and Fortin, M., 1991. Mixed and Hybrid Finite Element Methods, Spinger, New York.

[23] Hughes, T.J.R., 1995. Multiscale phenomena: Green´s function, Dirichlet-to Neumann formulation, subgrid scale models, bubbles and the origins of stabilized formulations, Comp. Meth. in Appl. Mech. and Eng., 127, 387-401.

[24] Hughes, T.J.R., Feijoó, G.R., Mazzei. L., Quincy, J.B., 1998. The variational multiscale method-a paradigm for computational mechanics, Comp. Meth. in Appl. Mech. and Eng., 166, 3-28.

[25] Codina, R. and Blasco, J., 1997. A finite element method for the Stokes problem allowing equal velocity-pressure interpolations, Comp. Meth. in Appl. Mech. and Eng., 143, 373-391.

[26] Codina, R., 2000. Stabilization of incompressibility and convection through orthogonal sub-scales in finite element methods, Comp. Meth. in Appl. Mech. and Eng., 190, 1579-1599.

[27] Hughes, T.J.R., Franca, L.P. and Balestra, M., 1986. A new finite element formulation for computational fluid dynamics: V. Circumventing the Babuska-Brezzi condition: A stable Petrov-Galerkin formulation of the Stokes problem accomodating equal-order interpolations. Comp. Meth. in Appl. Mech. and Eng., 59, 85-99.

[28] Jirásek, M. and Zimmermann, T. 1998. Analysis of Rotating Crack Model. Journal of Engineering Mechanics (ASCE), 124(8), 842-851.

[29] Simo, J.C., Oliver, J. and Armero, F. 1993. An analysis of strong discontinuities induced by strain-softening in rate-independent inelastic solids. Computational Mechanics, 12, 49-61.

[30] Jirásek, M. 2000. Comparative study on finite elements with embedded discontinuities. Comp. Meth. in Appl. Mech. and Eng., 188, 307-330.

[31] Mosler, J. and Meschke, G. 2003. 3D modelling of strong discontinuities in elastoplastic solids: fixed and rotating localization formulations. Int. J. Num. Meths. in Engng., 57, 1553-1576.

[32] Oliver, J., Huespe, A.E. Samaniego, E. and Chaves, W.V. 2004. Continuum approach to the numerical simulation of material failure in concrete. Int. J. for Num. and Anal. Meth. in Geomechanics.,28, 609-632.

[33] Oliver, J. and Huespe, A.E. 2004. Continuum approach to material failure in strong discontinuity settings. Comp. Meth. in Appl. Mech. and Eng., 193, 3195-3220.

[34] Mosler, J. 2005. A general technique to embed non-uniform discontinuities into standard solid finite elements. Computers and Structures, 84, 742-757.

[35] Manzoli, O.L. and Shing, P.B. 2006. On the efficient implementation of an elastoplastic damage model for large-scale analyses of material failure: a multiscale approach. Computers and Structures, 83, 369-382.

[36] Linder, C. and Armero, F. 2007. Finite elements with embedded strong discontinuities for the modeling of failure in solids. Int. J. Num. Meths. in Engng., 72, 1391-1433.

[37] Belytschko, T. and Black, T. 1999. Elastic crack growth in finite elements with minimal remeshing. Comp. Meth. in Appl. Mech. and Eng., 45(5), 601-620.

[38] Möes, N., Dolbow, J. and Belytschko, T. 1999. A finite element method for crack growth without remeshing. Int. J. Num. Meths. in Engng., 46, 131-150.

[39] Sukumar, N., Möes, N., Moran, B. and Belytschko, T. 2000. Extended finite element method for three-dimensional crack modelling. Int. J. Num. Meths. in Engng., 48, 1549-1570.

[40] Feist, C. and Hofstetter, G. 2006 . An embedded strong discontinuity model for cracking of plain concrete. Comp. Meth. in Appl. Mech. and Eng., 195, 7115-7138.

[41] Meschke, G. and Dumstorff, P. 2007 . Energy-based modeling of cohesive and cohesionless cracks via X-FEM. Comp. Meth. in Appl. Mech. and Eng., 196, 2338-2357.

[42] Patzák, B. and Jirásek, M. 2003. Process zone resolution by extended finite elements. Engineering Fracture Mechanics, 70, 957-977.

[43] Benvenuti, E., Tralli, A. and Ventura, G. 2008. A regularized XFEM model for the transition from continuous to discontinuous displacements. Int. J. Num. Meths. in Engng., 74, 911-944.

[44] Benvenuti, E. 2009. A regularized XFEM framework for embedded cohesive interfaces. Comp. Meth. in Appl. Mech. and Eng., 197, 4367-4378.

[45] Cervera, M. 2008. An orthotropic mesh corrected crack model. Comp. Meth. in Appl. Mech. and Eng., 197, 1603-1619.

[46] Cervera, M. 2008. A smeared-embedded mesh-corrected damage model for tensile cracking. Int. J. Num. Meths. in Engng., 76, 1930-1954.

[47] Sánchez, P.J., Sonzogni, V., Huespe, A. E., Oliver, J. 2006. Stabilized Mixed Finite Elements With Embedded Strong Discontinuities for Shear Band Modeling. J. of Applied Mechanics, ASCE, 73, 995-1003.

[48] Cervera, M., Agelet de Saracibar, C. and Chiumenti, M., 2002. COMET: COupled MEchanical and Thermal analysis. Data Input Manual, Version 5.0, Technical report IT-308, www.cimne.upc.es.

[49] GiD: The Personal Pre and Post Processor. 2011. Available from: <http://www.gidhome.com>.